scientific reports

Check for updates

OPEN

Exploration of the effect of multiple acceptor and π–spacer moieties coupled to indolonaphthyridine core for promising organic photovoltaic properties: a first principles framework

Mashal Khan[1,2], Muhammad Khalid[1,2]✉, Shahzad Murtaza[1,2], Ataualpa Albert Carmo Braga[3], Khalid Abdullah Alrashidi[4] & Sarfraz Ahmed[5]

Herein, the indolonaphthyridine-based molecules (INDTD1–INDTD8) with A_1–π–A_2–π–A_1 configuration were designed by the end-capped modification of INDTR reference with various acceptors. The density functional theory (DFT) and time-dependent DFT (TD-DFT) analyses at M06/6-31G(d,p) level were reported in this research to explore their optoelectronic and photovoltaic features. Their geometrical structures were initially optimized at the afore-said level and followed by various calculations such as the frontier molecular orbitals (FMOs), UV–Visible, density of states (DOS), transition density matrix (TDM), binding energy (E_b), open circuit voltage (V_{oc}) and fill factor (FF). Moreover, their global reactivity parameters (GRPs) were depicted by using the HOMO–LUMO band gaps obtained from the FMOs study. The tailored molecules demonstrated lower band gaps (2.183–2.269 eV) than INDTR (2.288 eV). They also showed bathochromic shifts in the visible region in chloroform (735.937–762.318 nm) and gas phase (710.384–729.571 nm) as compared to INDTR (724.710 and 698.498 nm, respectively). Further, intramolecular charge transfer (ICT) was demonstrated via the DOS and TDM graphical maps. Among all the entitled chromophores, INDTD7 showed significantly reduced band gap (2.183 eV), red-shifted absorption value (760.914 nm) in chloroform solvent and minimal E_b value (0.554 eV). The presence of –SO_3H groups on the terminal acceptors of INDTD7 may enhance the mobility of charges. The results suggested that the newly designed chromophores can be effective candidates for the future organic solar cell applications. Moreover, this study may encourage the experimentalists to develop photovoltaic materials.

Keywords DFT, Indolonaphthyridine, Non-fullerene acceptors, FMOs, Photovoltaics

Now a days, organic photovoltaic (OPV) solar cells are considered as light-weight, flexible, thin and efficient energy source which possess various applications in electronic fields[1]. The combined efforts of experimental and computational researchers have boosted their power conversion efficiency (PCE) up to 19.39% due to which they have been acknowledged as advanced solar energy devices[2]. Among the OPV devices, fullerenes are known as highly conjugated systems which heighten the mobility of charges. However they showed certain drawbacks such as structural instability, limited tuning of energy levels, undesirable morphology and poor light-absorption

[1]Institute of Chemistry, Khwaja Fareed University of Engineering & Information Technology, Rahim Yar Khan 64200, Pakistan. [2]Centre for Theoretical and Computational Research, Khwaja Fareed University of Engineering & Information Technology, Rahim Yar Khan 64200, Pakistan. [3]Departamento de Química Fundamental, Instituto de Química, Universidade de São Paulo, Av. Prof. Lineu Prestes, 748, São Paulo 05508-000, Brazil. [4]Department of Chemistry, College of Science, King Saud University, P.O. Box 2455, 11451 Riyadh, Saudi Arabia. [5]Harvard Medical School, Wellman Center for Photomedicine, Massachusetts General Hospital, Boston, MA 02114, USA. ✉email: muhammad.khalid@kfueit.edu.pk; Khalid@iq.usp.br

capability due to which their use becomes limited[3–5]. Consequently, the researchers have showed their interest toward the non-fullerene acceptors (NFAs) which are more efficient[6,7].

In comparison with fullerene-based counterparts, the NFAs-based materials exhibit a balance between optimal efficiency and cost stability. Moreover, they possess interesting molecular structures. Therefore, designing NFA compounds with low cost and synthetic complexity is a competitive choice for researchers[8]. Li et al. reported two NFAs (MO-IDIC and MO-IDIC-2F) which showed high photovoltaic performance for commercial applications[9]. Among them, MO-IDIC-2F exhibited 13.46% power conversion efficiency (PCE) which is favorable. The NFAs molecules with A–D–A′–D–A configuration are widely recognized as efficient light-harvesting devices and show high charge mobility. The side-chain engineering in them facilitates the intermolecular packing as well as maintains the solubility[10]. Efficient side-chain engineering of thieno-imidazole based compounds was reported to obtain profitable materials for organic solar cells by Areeba Asif et al. The compounds efficiently showed maximum absorbance (492–532 nm) and narrower energy gaps (1.76–1.99 eV). By comparative analysis, all the newly designed molecules showed enhanced photovoltaic attributes[11].

Indolonaphthyridine (IND) is one of the emerging electron-deficient chromophores which is highly planar. It is also known in literature as the bay-annulated indigo (BAI) as it was initially prepared by blocking the excited state deactivation of indigo dye via new rings formation at bay positions of the dye. This double bay-annulation reaction leads to formation of a compound named as cibalackrot[12]. The indolonaphthyridine-based derivatives showed several applications as they are utilized in organic lasers, photoacoustic imaging[13], transistors[14], singlet fission reactions[15], photodetectors and photovoltaics[16]. Their broad absorption in the near infrared (NIR) region of the electromagnetic spectrum rendered them good candidates to be utilized in transparent solar cell devices. Therefore, this research is highly grounded on the utilization of IND molecule.

It is observed in previous studies that the planar aromatic IND chromophore leads to poor solubility. To enable the solution processability, the solubilizing alkyl or aryl groups can be incorporated into this moiety. For this purpose, smaller groups based on thiophene and selenophene rings are considered as best choice which can effectively enable the solution processability[17,18]. Among the two (thiophene and selenophene rings), selenophene is the most appropriate choice for enhancing the device's performance. This is due to its interesting polar nature, quinoidal character which induces stronger Se-Se interactions and longer conjugation length[19].

Herein, new NFAs compounds (**INDTR** and **INDTD1**–**INDTD8**) are engineered utilizing the IND as the central core and accompanying the side chains composed of fused thiophenes (in case of **INDTR**) and selenophenes (in case of **INDTD1**–**INDTD8** derivatives). Further, the proposed molecules are distinguished via the proficient end-capping with extended malononitrile-type acceptors. The reason for the incorporation of acceptors and side chains (π–spacer) is to extend the conjugation length which leads to high charge mobility in the designed derivatives. To gain insights into their structure–property relationships, the density functional theory (DFT) is utilized and it is a computational approach which uses the electronic density of a system to determine its geometry and key electronic properties[20]. However, the excited-state properties are calculated by applying the time-dependent DFT (TD-DFT)[21]. Many common features such as charge mobility, reduced band gap and broader absorption are observed in all candidates. Their photovoltaic aspects are analyzed via detailed computational analyses to find out the best choice among all for organic solar cell (OSC) applications. To augment the features like open-circuit voltage (V_{oc}), a donor–acceptor interface is generated by using **PTB7** donor polymer. It is anticipated that the newly designed NFAs compounds will show remarkable potential for solar cells.

Methodology

The quantum chemical investigations were performed using the Gaussian 09 suite of program[22]. Initially, the structural optimization of the reference and newly designed molecules (**INDTR** and **IDTD1**–**INDTD8**) were performed at M06 level[23] of DFT in combination with 6-31G(d,p) basis set[24]. Their molecular configurations were viewed using the Gauss View 6.0 software[25]. The FMOs energies were viewed using the Avogadro software[26] to calculate their energy gaps. Further, the GRPs of the studied compounds were determined by utilizing their HOMO–LUMO band gaps. The time-dependent DFT (TD-DFT) analysis at the afore-said level was performed to calculate their UV–Visible spectra, FMOs and TDM. Moreover, the absorption spectra was obtained via the Origin 8.5 software[27]. The DOS analysis played significant role in showing the behavior of investigated compounds among the possible electronic states were drawn using the PyMOlyze software[28]. Similarly, the TDM maps which represented the excitation mobility among the atoms were obtained using the Multiwfn software[29] at the afore-said level. Other software programs such as Gauss Sum[30] and Chemcraft[31] were used to interpret the results from the output files.

Results and discussion

Designing of indolonaphthyridine-based chromophores

This study employs the quantum chemical investigation of novel fullerene-free acceptor compounds (**INDTR** and **INDTD1**–**INDTD8**) which aims to improve their photovoltaic performance by the end-capped modification[32]. The studied compounds, composed of A_1–π–A_2–π–A_1 configuration, are designed by utilizing the indolonaphthyridine (IND) moiety as the central core (A_2). Symmetric NFAs are proposed which possess the fused thiophene rings i.e., dithieno[3,2-b:2′,3′-d]thiophene-methane (1/1) as the π–spacer on both sides of IND core in case of **INDTR**, while in derivatives (**INDTD1**–**INDTD8**), more efficient selenophene rings i.e., diselenopheno[3,2-b:2′,3′-d]selenophene-methane (1/1) are incorporated as π-linkers instead of thiophenes. Their terminals are accommodated with extended acceptors (A_1) i.e., **MNM** in **INDTD1**; **FNM** in **INDTD2**; **CNM** in **INDTD3**; **BNM** in **INDTD4**; **CNT** in **INDTD5**; **CNC** in **INDTD6**; **CNS** in **INDTD7** and **NNM** in **INDTD8**. Figure 1 illustrates the strategy adopted for designing these chromophores. Table S11 shows their structures and IUPAC names. While, the IUPAC names of the overall molecules are shown in the Table S12 and their molecular

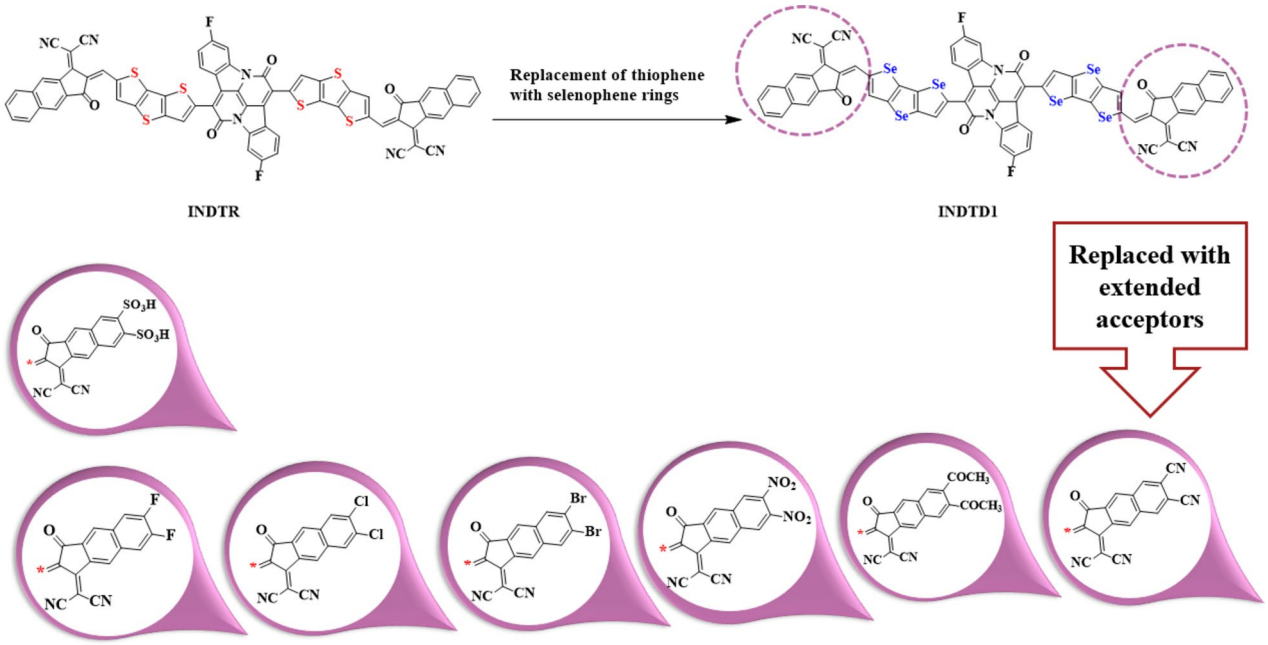

Figure 1. Schematic representation of designing of **INDTD1**–**INDTD8** from **INDTR**.

structures are displayed in the Fig. S1. The planarity parameters of the studied compounds are depicted by calculating their dihedral angles in various fragments. Their values largely depend on the nature of substituents involved in the compounds. The results are shown in Table S1. Four dihedral angles are calculated for each investigated molecule i.e., θ_1 is found between A_1 and π–spacer; θ_2 is reported between the A_2 and π–spacer; θ_3 is mentioned between A_2 and π–spacer; θ_4 is found between A_1 and π–spacer as shown in the Fig. 2 by using their optimized geometries. However, the side-view of their optimized structures are shown in the Fig. S2. The majority of derivatives except **INDTD6** show more negative and smaller values of θ_1 and θ_4 as compared to that of reference compound (**INDTR**). This depicts that the smaller and negative values of dihedral angles enhance the intramolecular charge transfer (ICT) in the designed molecules which shows their planar nature. However, the **INDTD6** compound has twisted or non-planar molecular nature as it shows positive and large values of θ_1 and θ_4[33]. Further, their Cartesian coordinates are collected in the Tables S2–S10.

Frontier molecular orbitals (FMOs) analysis

In frontier molecular orbital analysis, the highest occupied molecular orbital (HOMO) and lowest unoccupied molecular orbital (LUMO) are considered significant orbitals for understanding of the electronic properties. It has been widely used by organic chemists to understand the reactivity and regio-selectivity of various molecules[34,35]. The foremost application of FMOs analysis is the understanding of the Diels–Alder (DA) reaction which showed interaction between the FMOs of a diene and dienophile[36]. The HOMO–LUMO study is vital in predicting the reactive sites in conjugated frameworks[37]. Moreover, the energy gap (E_{gap}) between these orbitals characterizes the chemical stability and electronic conductivity as well as signifies the intramolecular charge transfer (ICT) amidst the electron donor and acceptor groups via the π–conjugated pathway[38]. Therefore, FMOs interpretation is crucial in quantum chemical analysis.

In the present work, the results of FMOs analysis are calculated at the M06/6-31G(d,p) level which are displayed in the Table 1. It is known that the efficiency of an OSC is determined from its energy band gap[39]. The proposed molecules successfully exhibit less energy gaps which show their potential to be utilized as OSC in future. The E_{HOMO} and E_{LUMO} values for the reference compound (**INDTR**) are – 5.793 and – 3.505 eV, respectively. Moreover, it shows energy gap as 2.288 eV which is the highest among all compounds. Similarly, in case of the designed derivatives (**INDTD1**–**INDTD8**), E_{HOMO} values are – 5.766, – 5.794, – 5.816, – 5.814, – 5.892, – 5.817, – 5.898 and – 5.905 eV, correspondingly. While, their E_{LUMO} are – 3.506, – 3.539, – 3.579, – 3.576, – 3.705, – 3.583, – 3.715 and – 3.729 eV, respectively. Further, their E_{gap} values are 2.260, 2.255, 2.237, 2.238, 2.187, 2.234, 2.183 and 2.190 eV, respectively. The some other orbital energies (HOMO-1/LUMO + 1 and HOMO-2/LUMO + 2) are also calculated which are presented in the Table S13.

It is known from the literature analysis that a photovoltaic material which possesses less band gap will show high PCE as an OSC material[40]. Herein, the electronic nature of the proposed molecules is estimated which shows that all derivatives exhibit closer energy gaps which are slightly lesser than **INDTR** reference. The compound (**INDTD7**) shows the least energy gap as 2.183 eV which is attributed to the strong terminal acceptor i.e., **CNS**. The introduction of sulphonic acid group (–SO_3H) minimizes the energy gap, promote the charge transfer, separates the interface charges and inhibit the hole-electron recombination[41]. Due to its significance, the acceptor of **INDTD7** is regarded highly efficient and overall molecule seems to be the reasonable candidate for OSC devices. Moreover, the compound (**INDTD5**) which has **CNT** end-capped acceptor shows slightly higher band gap (2.187 eV) than **INDTD7**. This band gap is further elevated in case of **INDTD8** (2.190 eV) which

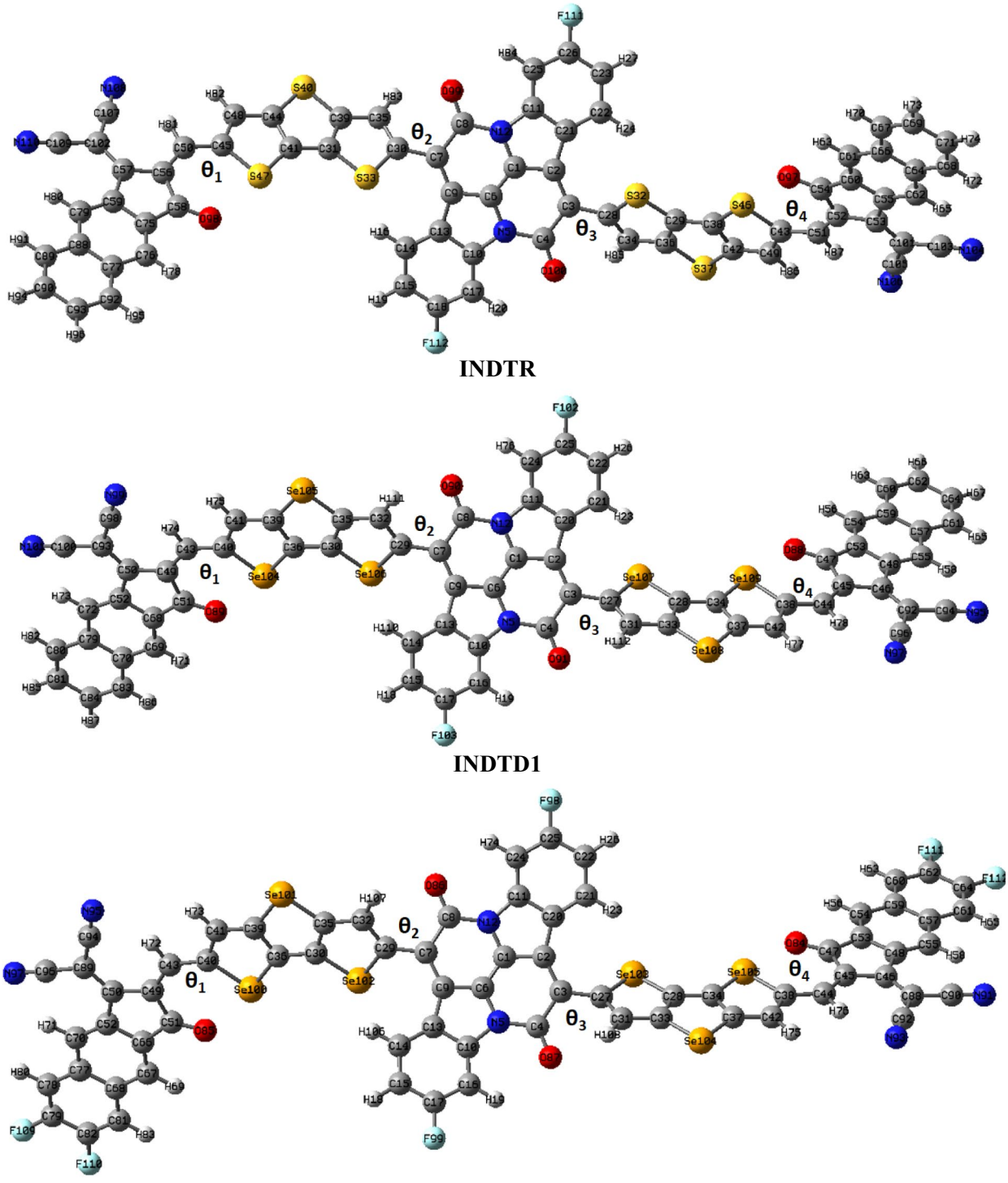

Figure 2. Optimized structures of the entitled chromophores (**INDTR** and **INDTD1–INDTD8**).

contains **NNM** acceptor at its terminal. Since, $-SO_3H$, –CN and $-NO_2$ groups show negative mesomeric effect (*–M* effect) as well as inductive effect (*–I* effect), hence, closer values of E_{gap} are observed in **INDTD7**, **INDTD5** and **INDTD8**, respectively.

The compounds (**INDTD1–INDTD4** and **INDTD6**) show higher band gaps in the range of 2.234–2.288 eV. In case of **INDTD6**, the band gap of 2.234 eV is observed which is due to the presence of **CNC** acceptor moiety. Similarly, in case of **INDTD3** and **INDTD4**, higher band gaps of 2.237 and 2.238 eV are observed owing to the presence of **CNM** and **BNM** acceptors, respectively. Lastly, the derivatives (**INDTD1** and **INDTD2**) show comparable E_{gap} as 2.260 and 2.255 eV as they possess **MNM** and **FNM** terminal acceptors, respectively. Overall, a

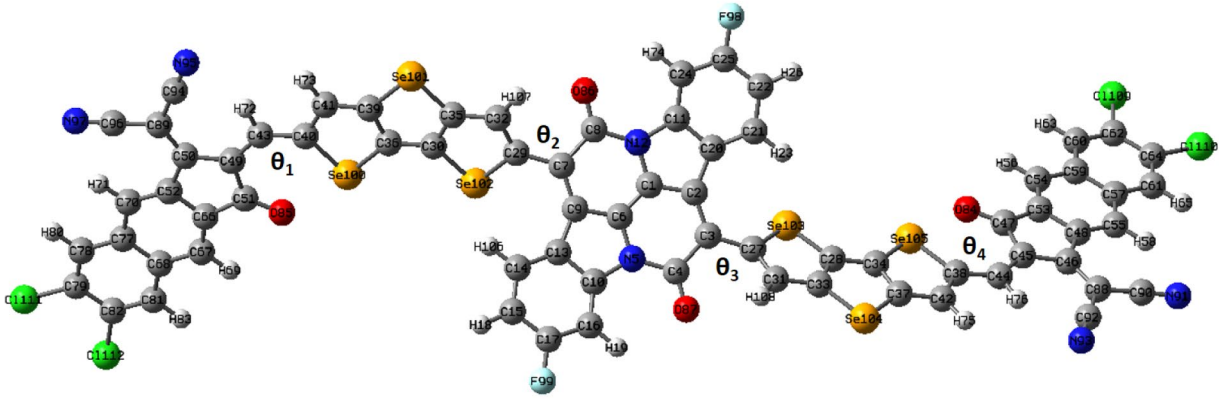

INDTD3

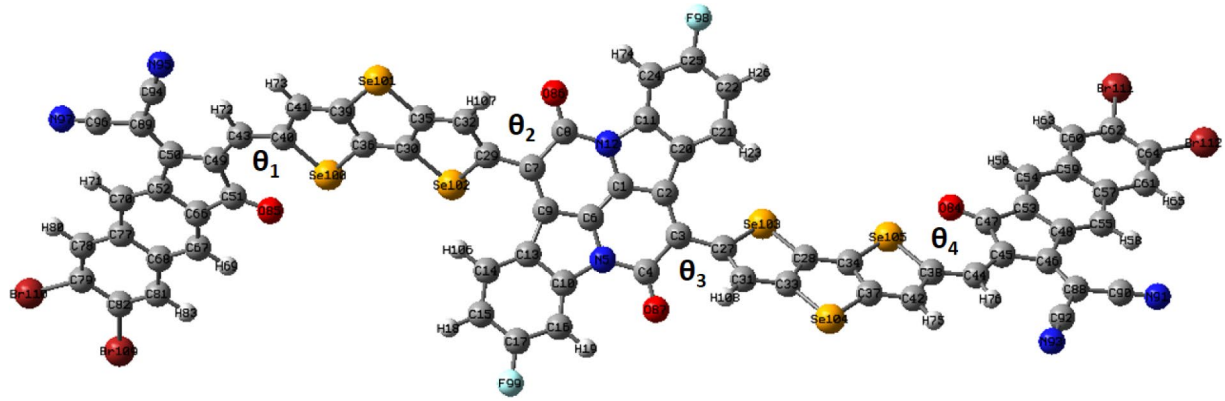

INDTD4

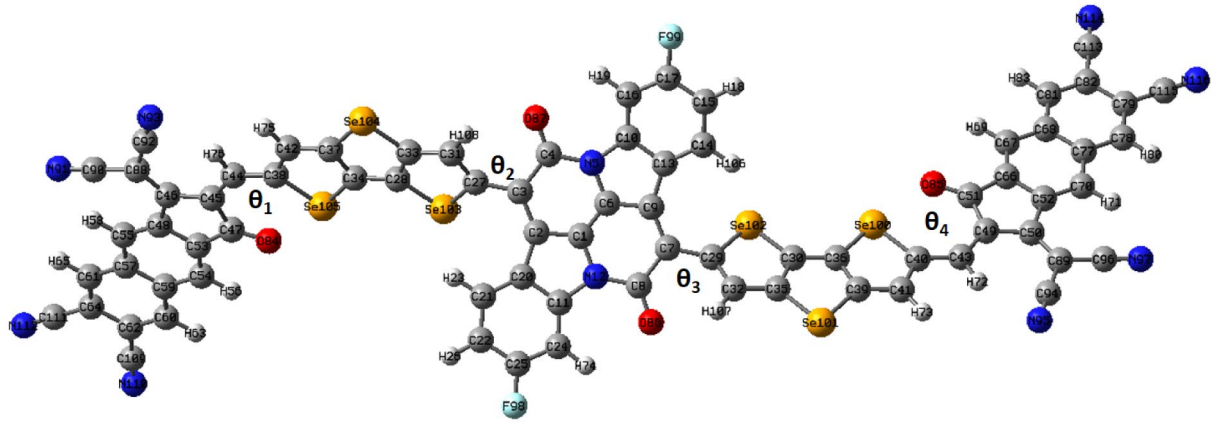

INDTD5

Figure 2. (continued)

following increasing order is observed for E_{gap}: **INDTD7 < INDTD5 < INDTD8 < INDTD6 < INDTD3 < INDTD4 < INDTD2 < INDTD1 < INDTR**.

From the FMOs diagrams, it is observed that the electronic clouds in case of HOMOs are majorly concentrated over the π–linkers and 1,5-dihydro-1,5-naphthyridine-2,6-dione (NTD) portion of the central acceptor core and NTD is widely known as a component of n-type organic semiconductors[42]. Moreover, a minor HOMO density is also seen over the terminal acceptors. In case of LUMOs, the electron density is highly concentrated over the central acceptor (IND) and end-capped acceptors in all the titled chromophores. While, a few clouds are also seen over the π–linkers. Figure 3 demonstrates the FMOs surface plots for **INDTR** and **INDTD1–INDTD8** compounds. Similarly, the orbital surfaces of HOMO-1/LUMO + 1 and HOMO-2/LUMO + 2 are shown in the Fig. S3.

Hence, it is inferred from the above discussion that the major charge density for HOMO is concentrated over the bridging units and for LUMO, it is located over the acceptor components. Moreover, the lower band gaps of the titled chromophores indicate a massive ICT in them. So, they are regarded as effective for solar cell applications.

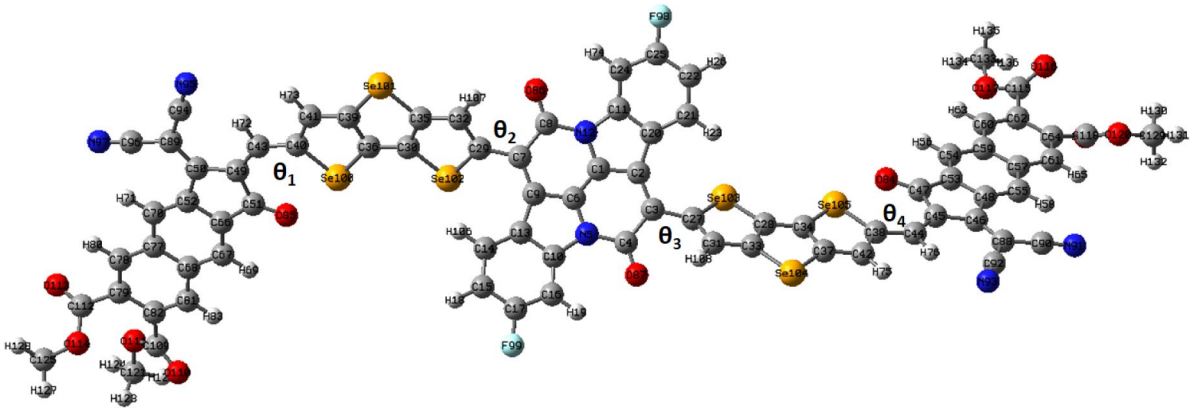

INDTD6

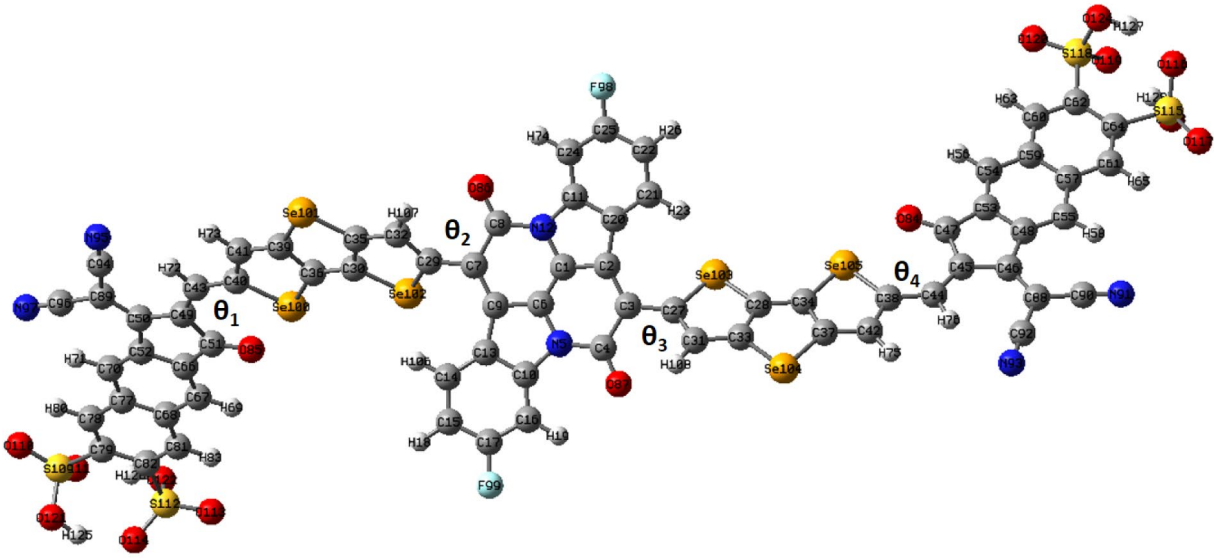

INDTD7

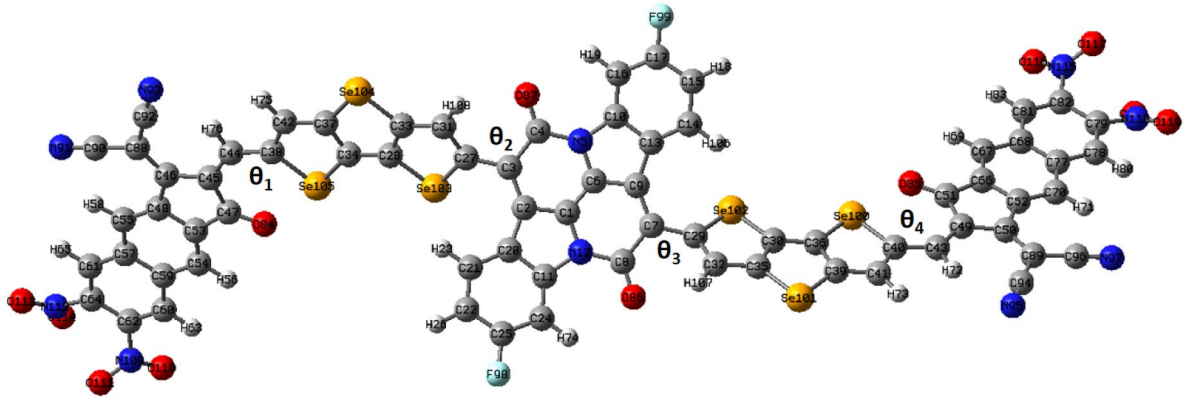

INDTD8

Figure 2. (continued)

Global reactivity parameters (GRPs)

To assess the stability and reactivity of the investigated chromophores, their global reactivity parameters (GRPs) are evaluated. These are electronegativity (X)[43], chemical potential (μ)[44], chemical hardness (η)[45], chemical softness (σ)[46], electrophilicity index (ω)[47], ionization potential (IP)[48], electron affinity (EA)[49] and electronic charge transfer (ΔN_{max}). For the sake of their analysis, HOMO–LUMO band gap is utilized. The Eqs. (S1)–(S8) aid in theoretical calculations of GRPs for the **INDTR** and **INDTD1–INDTD8** compounds. The values obtained in eV are displayed in the Table 2.

Compounds	E_{HOMO}	E_{LUMO}	E_{gap}
INDTR	−5.793	−3.505	2.288
INDTD1	−5.766	−3.506	2.260
INDTD2	−5.794	−3.539	2.255
INDTD3	−5.816	−3.579	2.237
INDTD4	−5.814	−3.576	2.238
INDTD5	−5.892	−3.705	2.187
INDTD6	−5.817	−3.583	2.234
INDTD7	−5.898	−3.715	2.183
INDTD8	−5.905	−3.729	2.190

Table 1. Energies of the frontier molecular orbitals of **INDTR** and **INDTD1–INDTD8**. Units are reported in eV.

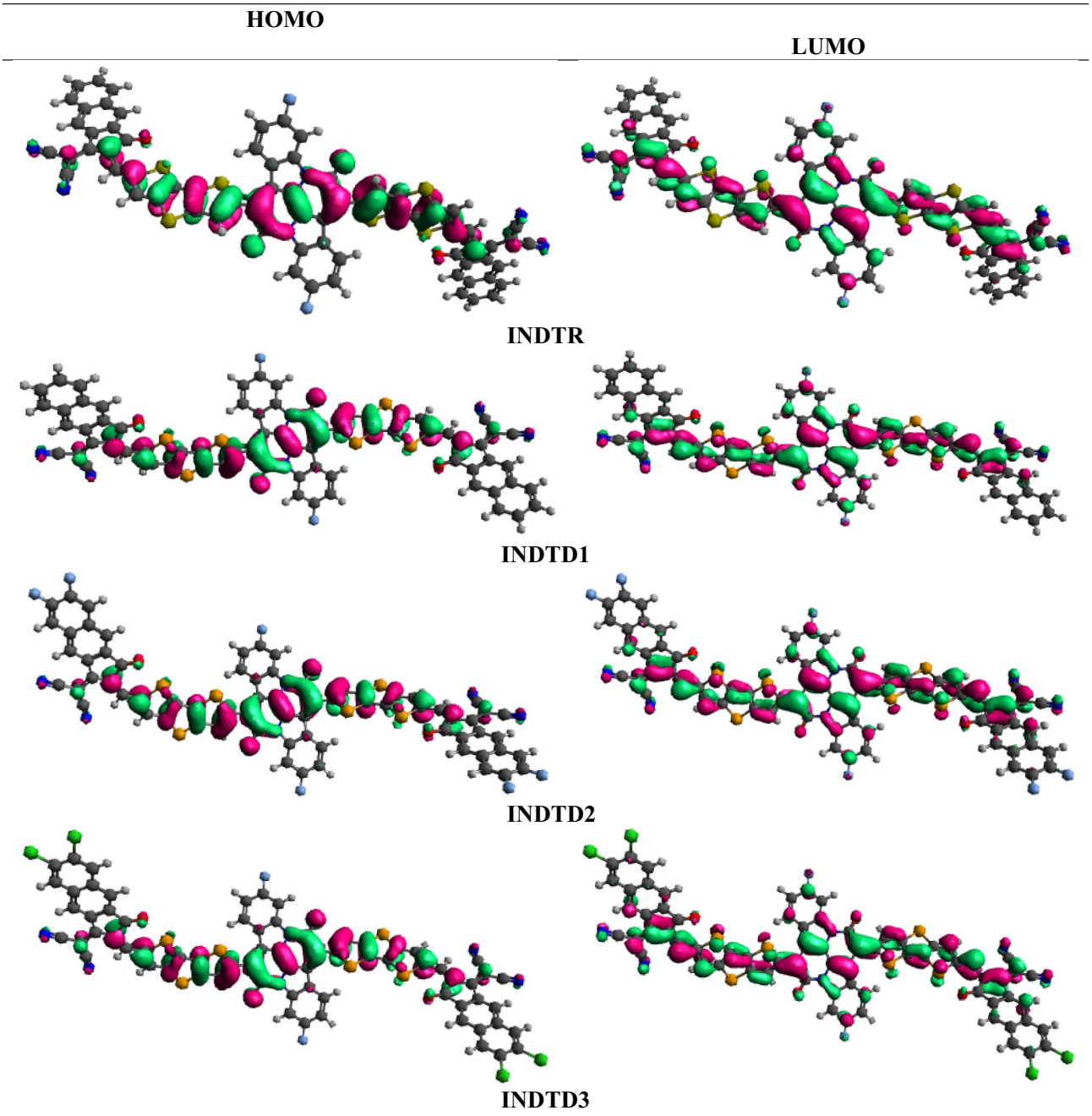

Figure 3. Illustration of FMOs (HOMOs and LUMOs) of **INDTR** and **INDTD1–INDTD8**.

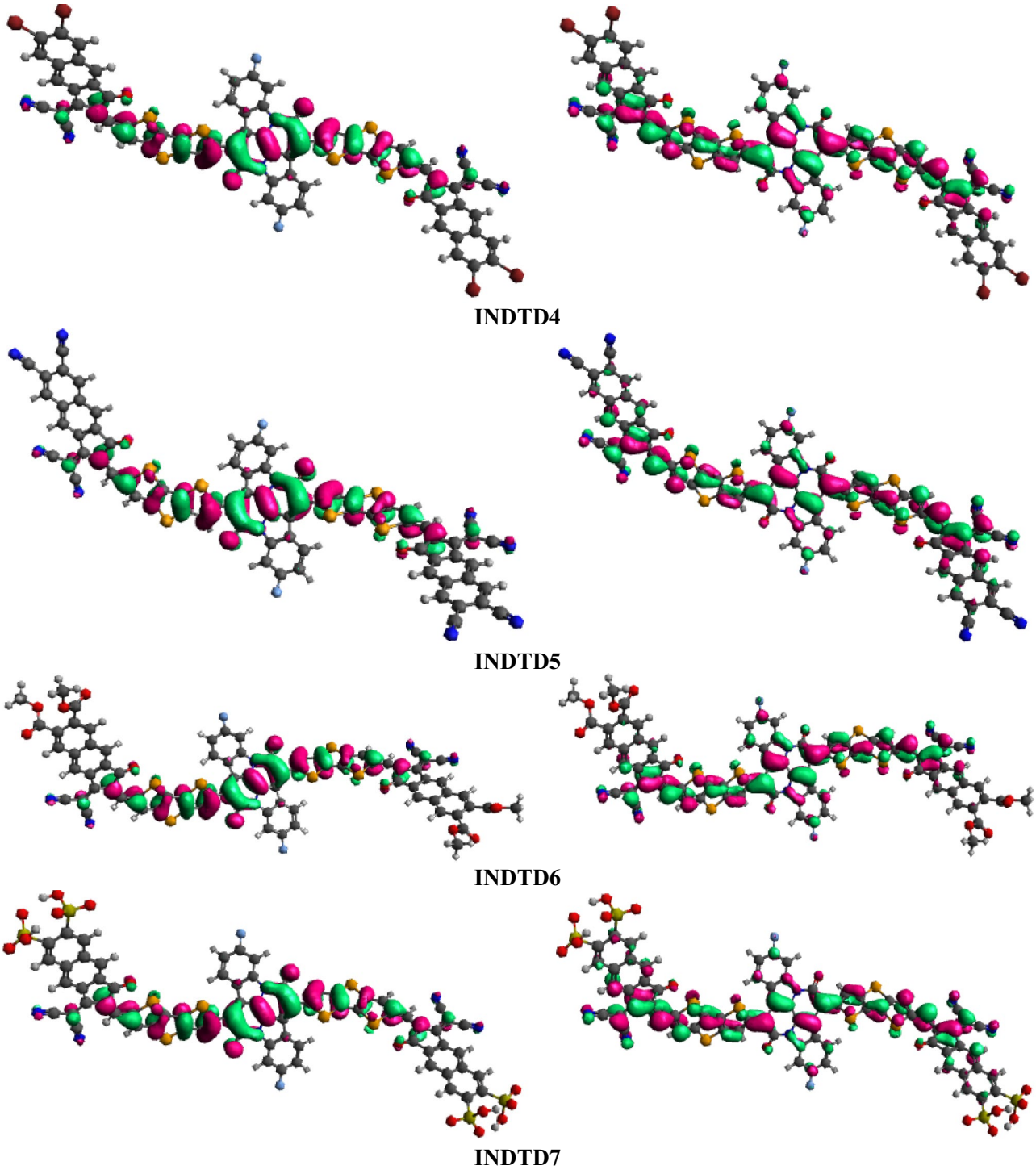

Figure 3. (continued)

The results referred in the Table 2 indicate that among all candidates, **INDTD5**, **INDTD7** and **INDTD8** are the most electronegative compounds with values of X as 4.799, 4.807 and 4.810 eV, respectively. Moreover, their acceptor nature is further confirmed via minimum chemical potential (μ) values as − 4.799, − 4.807 and − 4.810 eV, respectively which also confirms the highest charge transfer (CT)[50]. In order to predict their reactivity, global hardness (η) and global softness (σ) are significant parameters which are inversely related to each other. Molecules with higher values of σ and lower values of η show least HOMO–LUMO energy gap, least stability and utmost reactivity[51]. Interestingly, maximum values of σ are obtained for the above-mentioned chromophores as 0.457, 0.458 and 0.457 eV^{-1}, accordingly. Contrarily, minimum η values for **INDTD5**, **INDTD7** and **INDTD8** are 1.094, 1.092 and 1.095 eV, respectively.

Other intriguing properties are electrophilicity index (ω) and electronic charge transfer (ΔN_{max}) both of which determine the molecules' ability to absorb electronic charge from the environment[52]. Molecules with higher

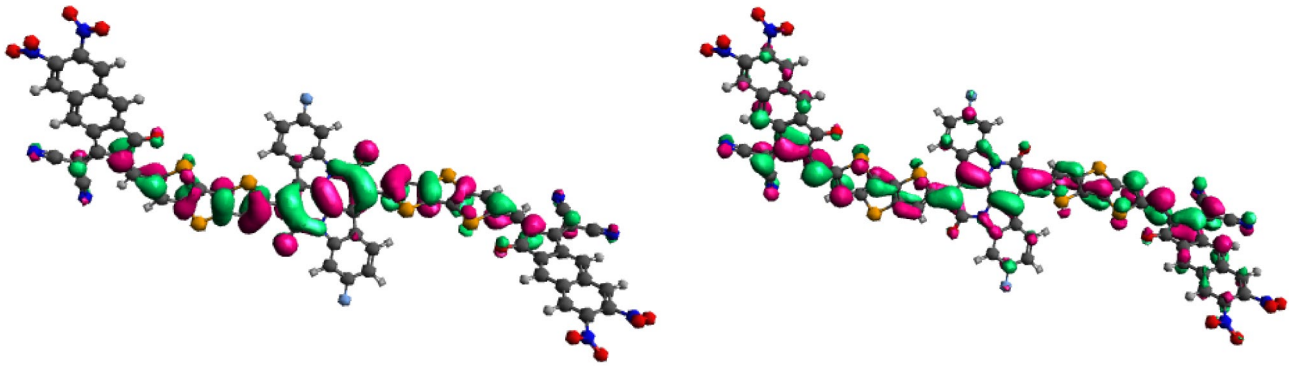

INDTD8

Figure 3. (continued)

Compounds	*X*	*μ*	*η*	*σ*	*ω*	*IP*	*EA*	ΔN_{max}
INDTR	4.649	−4.649	1.144	0.437	9.446	5.793	3.505	4.064
INDTD1	4.636	−4.636	1.130	0.442	9.600	5.766	3.506	4.103
INDTD2	4.667	−4.667	1.128	0.443	9.657	5.794	3.539	4.137
INDTD3	4.698	−4.698	1.119	0.447	9.864	5.816	3.579	4.198
INDTD4	4.695	−4.695	1.119	0.447	9.849	5.814	3.576	4.196
INDTD5	4.799	−4.799	1.094	0.457	10.528	5.892	3.705	4.387
INDTD6	4.700	−4.700	1.117	0.448	9.888	5.817	3.583	4.208
INDTD7	4.807	−4.807	1.092	0.458	10.583	5.898	3.715	4.405
INDTD8	4.810	−4.810	1.095	0.457	10.564	5.905	3.715	4.393

Table 2 . Ionization potential (*IP*), electron affinity (*EA*), electronegativity (*X*), chemical potential (μ), global hardness (η), global softness (σ) and global electrophilicity (ω). Units are in eV. Global softness (σ) in eV^{-1}.

values of these parameters are likely to act as an electrophile and vice versa[53]. It is observed for the currently studied chromophores that highest values of ω and ΔN_{max} are obtained for **INDTD5**, **INDTD7** and **INDTD8** among all. Their $\omega = 10.528$, 10.583 and 10.564 eV and $\Delta N_{max} = 4.387$, 4.405 and 4.393 eV, respectively. Furthermore, the electron affinity (*EA*) and ionization potential (*IP*) are indicative of their redox potentials and show highest values for the afore-said designed molecules $IP = 5.892$, 5.898 and 5.905 eV, while $EA = 3.705$, 3.715 and 3.715 eV, respectively[54]. Concluding the discussion, the proposed molecules tend to be the reasonable solar cell candidates.

UV–Visible analysis

To estimate the optical properties of the studied chromophores (**INDTR** and **INDTD1–INDTD8**), their UV–Visible analysis is performed at the afore-mentioned level of TD-DFT i.e., M06/6-31G(d,p) level in gas and solvent (chloroform) phases. This includes the interpretation of absorption wavelength (λ_{max}), oscillator strength (f_{os}), excitation energy (*E*) and molecular orbital assessments of the titled compounds[55]. The molecules which depict high oscillation frequency along with intense absorption bands are rendered as suitable candidates for solar cell utility owing to their efficient charge transfer[56]. Table 3 shows the representative values of absorption wavelengths (λ_{max}) along with their corresponding features for all the proposed molecules. While, Tables S14–S31 mentioned in the supplementary information show other values for individual compounds. Figure 4 demonstrates the UV–Visible spectra for the titled chromophores.

The data mentioned above clearly shows that the absorption maxima (λ_{max}) of designed compounds (**INDTD1–INDTD8**) are significantly higher than the reference compound (**INDTR**). The reason is the end-capped substitution in the derivatives with extended acceptors which possess electron-withdrawing substituents. The absorption maxima of designed derivatives lie in the visible region in chloroform (735.937–762.318 nm) as well as in the gaseous phase (710.384–729.571 nm).

The key optical characteristics such as absorption maxima, oscillator strengths and overall optical properties are greatly influenced by the solvent's environment. Polar solvents tend to stabilize the excited states of chromophores more than non-polar solvents, causing a red shift, where the absorption peak shifts to longer wavelengths. Conversely, a blue shift is dictated by non-polar solvents where the absorption peak shifts to shorter wavelengths due to lesser stabilization of the excited states. The oscillator strengths (f_{os}) are influenced by the interaction of solvent's viscosity and polarity which plays a key role in determining the transition probabilities in a molecule. A higher viscosity changes the solvent's dielectric constant and refractive index which may prolong the optical gain, altering the linear optical properties[57]. Thus, the solvent characteristics can either enhance or diminish transition probabilities in the absorbing molecules. The overall optical properties of solute molecules including the absorption spectra and emission characteristics are greatly influenced by the solvent used. Specific solute–solvent

	System	TD-DFT λ_{max} (nm)	E (eV)	f_{os}	MO contributions
Phase[a]	INDTR	698.498	1.775	2.607	H→L (95%), H-1→L+1 (4%)
	INDTD1	710.384	1.745	2.617	H→L (95%), H-1→L+1 (4%)
	INDTD2	711.607	1.742	2.642	H→L (95%), H-1→L+1 (4%)
	INDTD3	717.330	1.728	2.714	H→L (94%), H-1→L+1 (4%)
	INDTD4	717.164	1.729	2.717	H→L (94%), H-1→L+1 (4%)
	INDTD5	729.056	1.701	2.742	H→L (94%), H-1→L+1 (4%)
	INDTD6	716.998	1.729	2.698	H→L (94%), H-1→L+1 (4%)
	INDTD7	729.400	1.700	2.726	H→L (94%), H-1→L+1 (4%)
	INDTD8	729.571	1.699	2.694	H→L (94%), H-1→L+1 (4%)
Phase[b]	INDTR	724.710	1.711	2.851	H→L (94%), H-1→L+1 (4%)
	INDTD1	735.937	1.685	2.869	H→L (93%), H-1→L+1 (5%)
	INDTD2	738.084	1.680	2.885	H→L (93%), H-1→L+1 (5%)
	INDTD3	745.003	1.664	2.943	H→L (93%), H-1→L+1 (5%)
	INDTD4	744.689	1.665	2.940	H→L (93%), H-1→L+1 (5%)
	INDTD5	760.354	1.631	2.958	H→L (92%), H-1→L+1 (5%)
	INDTD6	745.720	1.663	2.917	H→L (93%), H-1→L+1 (5%)
	INDTD7	760.914	1.629	2.938	H→L (92%), H-1→L+1 (5%)
	INDTD8	762.318	1.626	2.909	H→L (91%), H-1→L+1 (5%)

Table 3. Wavelength (λ_{max}), excitation energy (E), oscillator strength (f_{os}) and major molecular orbital assessments of compounds (**INDTR** and **INDTD1–INDTD8**) in gaseous and solvent phases. [a]Gaseous Phase. [b]Chloroform Solvent.

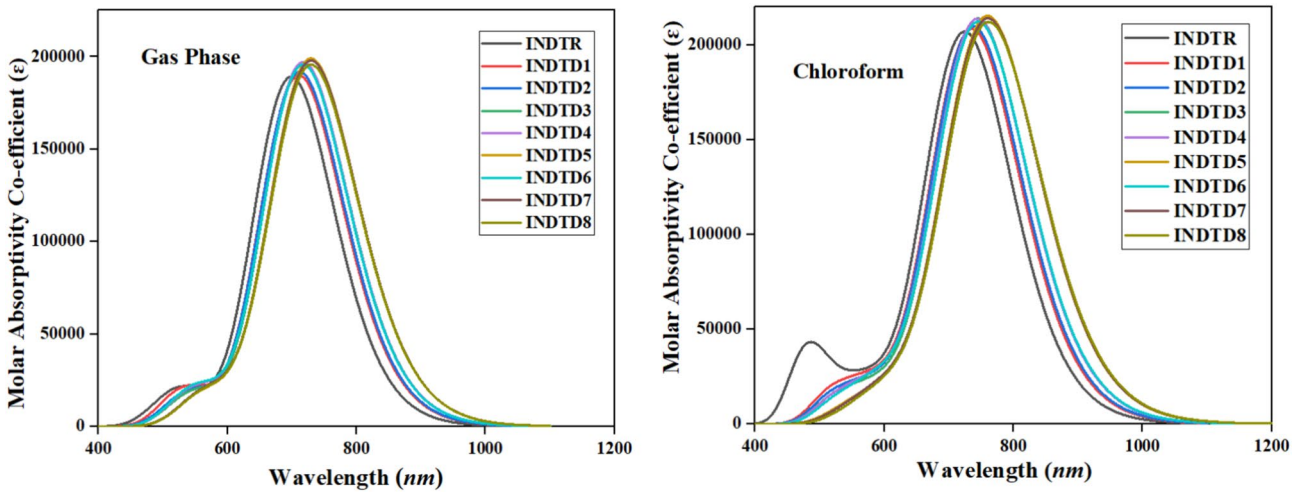

Figure 4. UV–Vis plots for the investigated chromophores.

interactions can also modify the solute's electronic states, resulting in varied absorption characteristics. For example, the absorption peak intensities increase via the hydrogen bonding between polar solvents and solutes[58].

Chloroform is known as the moderately polar solvent in theoretical UV–Vis spectroscopy for several reasons such as low UV absorption. This ensures its minimal interference with the absorption bands of the studied compounds. Moreover, chloroform is transparent to UV–Visible light over a wide range of wavelengths, which allows for accurate measurement of absorbance for the studied compounds without background interference from the solvent. It also shows good solubility for many organic compounds and is relatively stable. Furthermore, it is non-reactive towards many organic molecules and is easy to handle which makes it a preferred choice for this study[59]. Overall, the chloroform phase demonstrates more prominent results as compared to the gas phase.

In gaseous phase, the reference compound (**INDTR**) shows λ_{max} = 698.498 nm with excitation energy (E) as 1.775 eV. The oscillation strength (f_{os}) of **INDTR** is 2.607 along with H → L transition of 95%. The derivatives (**INDTD1–INDTD8**) show λ_{max} as 710.384, 711.607, 717.330, 717.164, 729.056, 716.998, 729.400 and 729.571 nm, respectively. They show correspondingly lower E as 1.745, 1.742, 1.728, 1.729, 1.701, 1.729, 1.700 and 1.629 eV. Moreover, their f_{os} are depicted as 2.617, 2.642, 2.714, 2.717, 2.742, 2.698, 2.726 and 2.694, accordingly. Furthermore, all derivatives show H → L transition as 94% except **INDTD1** and **INDTD2** which show 95% contribution. Overall, the investigated chromophores show the following increasing trend for the absorption

maxima (λ_{max}) in the gaseous phase in nm: **INDTR < INDTD1 < INDTD2 < INDTD6 < INDTD4 < INDTD3 < INDTD5 < INDTD7 < INDTD8**.

For chloroform, the λ_{max} values for the investigated compounds are higher than gaseous phase which are as follows: 724.710, 735.937, 738.084, 745.003, 744.689, 760.354, 745.720, 760.914 and 762.318 nm for **INDTR** and **INDTD1–INDTD8**, correspondingly. Similarly, their excitation energy values are lower than those obtained in gaseous phase: 1.711, 1.685, 1.680, 1.664, 1.665, 1.631, 1.663, 1.629 and 1.626 eV for **INDTR** and **INDTD1–INDTD8**, respectively. Moreover, they show oscillation strengths as 2.851, 2.869, 2.885, 2.943, 2.940, 2.958, 2.917, 2.938 and 2.909, respectively. The H → L transitions show 94% for **INDTR**, 93% for **INDTD1–INDTD4** and **INDTD6**, 92% for **INDTD7** and 91% for **INDTD8** compound. The λ_{max} in case of chloroform solvent are obtained in the following increasing trend for the absorption maxima (λ_{max}) in gaseous phase in nm: **INDTR < INDTD1 < INDTD2 < INDTD4 < INDTD3 < INDTD6 < INDTD5 < INDTD7 < INDTD8**. The results suggested that **INDTD7** and **INDTD8** compounds show the red-shifted absorption values as compared to other derivatives. Hence, they are considered as reasonable candidates for solar cell devices.

Charge transfer (CT) analysis

The charge transfer analysis is performed by utilizing the NFA compound (**INDTD7**) in conjugation with the selected donor polymer (**PTB7**) as can be seen in Fig. 5.

For the present study, **PTB7** donor polymer is incorporated with **INDTD7** compound to form the donor:acceptor complex which is shown in the Fig. 6. Among all the derivatives, **INDTD7** is utilized to observe the charge transfer phenomena owing to its least energy gap and highest bathochromic shift. The Fig. 6 shows that the charge coherence is largely concentrated over the HOMO for **PTB7** and in case of **INDTD7**, the LUMO shows dominant charge density. Thus, it is clearly observed that the ample charge transfer is seen via the HOMO to LUMO among the donor:acceptor complex.

Density of states (DOS)

Density of State is a valuable tool for analyzing the charge distribution around HOMOs and LUMOs of the examined compounds and assists in verifying the findings of FMOs[60]. This study is often conducted to forecast the percentage contribution of each component of a molecule to the overall distribution of electronic charges and facilitates in the determination of intramolecular charge transfer[61]. In a DOS map, the HOMO region of a compound is represented by left side energy values, while the LUMO region is represented by right side energy values along the x-axis. The central area between these two regions is the energy gap and is similar to the band-gap of FMOs[62]. To explicate the DOS analysis, the studied chromophores are fragmented into the Acceptor-1 (peripheral acceptor unit), Acceptor-2 (core unit) and the π–spacer. These fragments are represented by blue, red and green lines, respectively, as illustrated in the Fig. 6.

Moreover, this study reveals that electrons are distributed from HOMO, which has a high capacity for donation, to LUMO, which prefers to accept them[63]. The modification of peripheral acceptor moieties alters the pattern of charge distribution, as indicated by the HOMO–LUMO percentages of DOS displayed in the Table S32. In this study, Acceptor-2 corresponds to 39.5, 38.9, 39.5, 39.9, 39.9, 41.6, 40.1, 42.1 and 42.0% for the HOMO, while 44.7, 42.9, 40.7, 38.2, 38.0, 30.2, 37.1, 29.5, and 27.9% for the LUMO in **INDTR** and **INDTD1–INDTD8**, accordingly. Similarly, the π–spacer contributes 45.9, 46.5, 46.0, 45.5, 45.5, 44.0, 45.4, 43.6 and 43.7% towards the HOMO and 25.4, 27.5, 27.7, 28.0, 27.9, 28.1, 27.9, 28.3, and 27.5% towards the LUMO for **INDTR** and **INDTD1–INDTD8**, respectively. Further, the terminal Acceptor-1 exhibits distribution percentages of 14.6, 14.6, 14.5, 14.6, 14.6, 14.4, 14.5, 14.3, and 14.3% for the HOMO, while 29.9, 29.6, 31.6, 33.8, 34.1, 41.7, 35.0, 42.1 and 44.6% for the

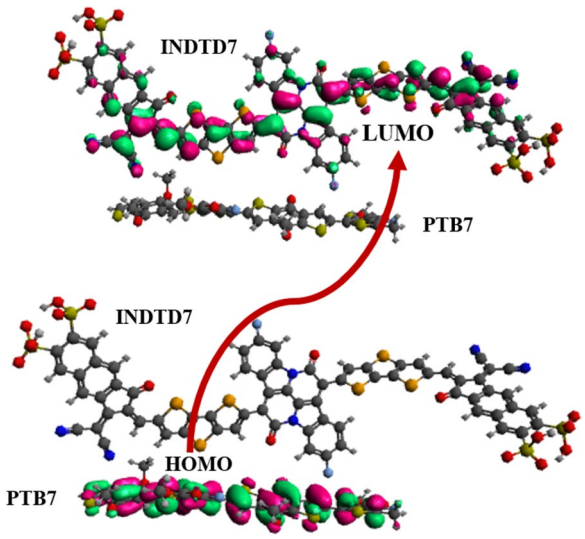

Figure 5. Charge transfer analysis for **PTB7** (donor): **INDTD7** (acceptor) complex.

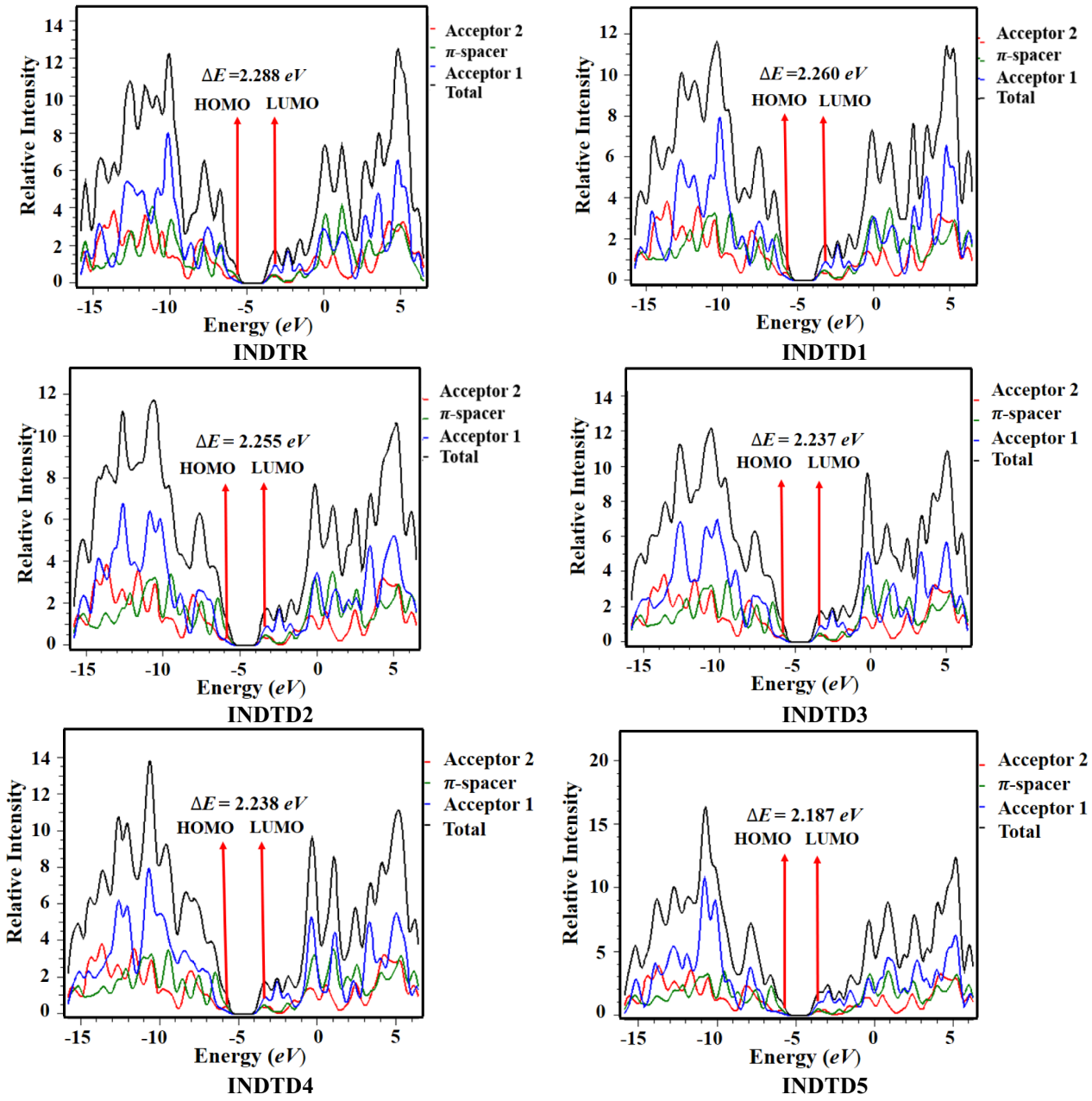

Figure 6. DOS pictographs of **INDTR** and **INDTD1–INDTD8**.

LUMO in **INDTR** and **INDTD1–INDTD8**, correspondingly. According to the preceding discussion, the highest charge density in HOMOs is localized over the selenophene based π–spacer as well as over central Acceptor-2 of all designed chromophores, whereas the charge density in LUMOs is mostly centered over the Acceptor-1. Furthermore, these π–spacer play a crucial role in the charge transfer process. In a nutshell, the DOS graphs show that a significant charge from the central Acceptor-2 towards the terminal Acceptor-1 is shifted via the selenophene bridges in all the investigated compounds.

Transition density matrix (TDM)

TDM is an efficient tool which provides qualitative details about the 2-D movement of electrons, exciton dynamics and the extent of coherence within conjugated molecular structures[64]. It also investigates the nature of transitions particularly from the ground state (S_0) to excited state (S_1), degree of delocalization within the molecules as well as the interaction between charge donating and accepting moieties throughout the transition[65]. The TDM plots for **INDTR** and **INDTD1–INDTD8** are generated using the TD-DFT computations at M06/6-31G(d,p) functional and the results are illustrated by using the Multiwfn software. The influence of hydrogen atoms is disregarded due to their minimal impact in transitions. In these TDM graphs, the bottom x-axis represents the number of individual atoms, while the density of individual electrons is depicted by color bars on the right y-axis.

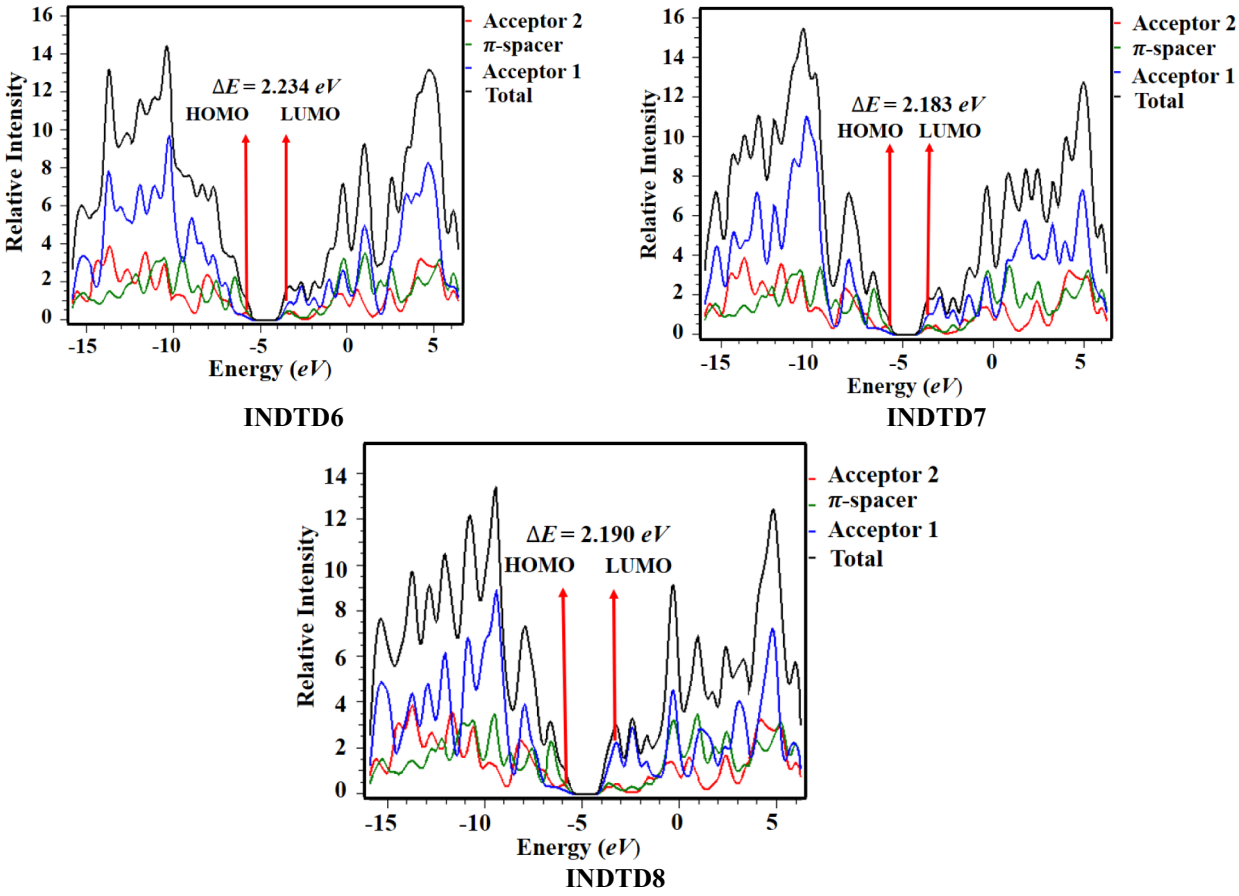

Figure 6. (continued)

To have a better understanding, the molecules are categorized into three fragments: end-capped acceptor (A1), core acceptor (A2) and the π–spacer. All molecules (**INDTR** and **INDTD1**–**INDTD8**) exhibit charge transformation from the central core (A2) towards the terminal charge accepting (A1) moieties. The π-linker unit facilitates this process without causing any interference. It is observed that charge density is primarily localized on the central A2 unit, moderately distributed on the π–spacer and shows minimal coherence at the terminal A1 unit in all studied compounds in both diagonal and off-diagonal regions. Moreover, substantial charge scattering occurs along the diagonal paths (see Fig. 7). The increasing order of interaction coefficients for charge donating and accepting units is found as: **INDTD7 < INDTD5 < INDTD8 < INDTD6 < INDTD4 = INDTD3 < INDTD2 = INDTD1 < INDTR**. Due to lesser hole–electron coupling, **INDTD7** has a lower coefficient of interaction than other modified compounds and exhibits more substantial exciton dissociation in the excited state. This allows for faster excitation and elevated charge transmission rate. The interaction coefficient of **INDTD7** is comparable to that of **INDTD5**. This is due to the fact that **INDTD5** also has lower coupling of exciton which may lead to greater charge dissociation rate. Consequently, all designed compounds reveal momentous charge dissociation than the **INDTR** compound. This implies that the studied compounds (**INDTR** and **INDTD1**–**INDTD8**) are versatile and unique which are capable of developing good OSCs.

Exciton binding energy (E_b)

The exciton dissociation energy (EDE) is a crucial factor in determining the efficiency of photovoltaic devices. It is the amount of energy needed to separate excitons into holes and electrons. The columbic force between holes and electrons is calculated by determining the binding energies of the investigated compounds. A smaller value of E_b indicates weaker columbic interactions and a significant charge transfer[66]. The Eq. (1)[67] is used to calculate the E_b values and the outcomes are shown in the Table 4.

$$E_b = E_{gap} - E_{opt}. \quad (1)$$

It is noted that the exciton binding energy (E_b) is the difference between the energy gap (E_{gap}) and the first excitation energy (E_{opt}). Here, E_{gap} represents the bandgap between the HOMO and LUMO, while E_{opt} signifies the minimum energy required for the first excitation[67–69].

The E_b values of **INDTR** and **INDTD1**–**INDTD8** are 0.577, 0.575, 0.575, 0.573, 0.573, 0.556, 0.571, 0.554 and 0.564 eV, respectively. The escalating trend of E_b for all the studied compounds is as follows: **INDTD7 < INDTD5 < INDTD8 < INDTD6 < INDTD4 = INDTD3 < INDTD2 = INDTD1 < INDTR**. It is noted that compounds

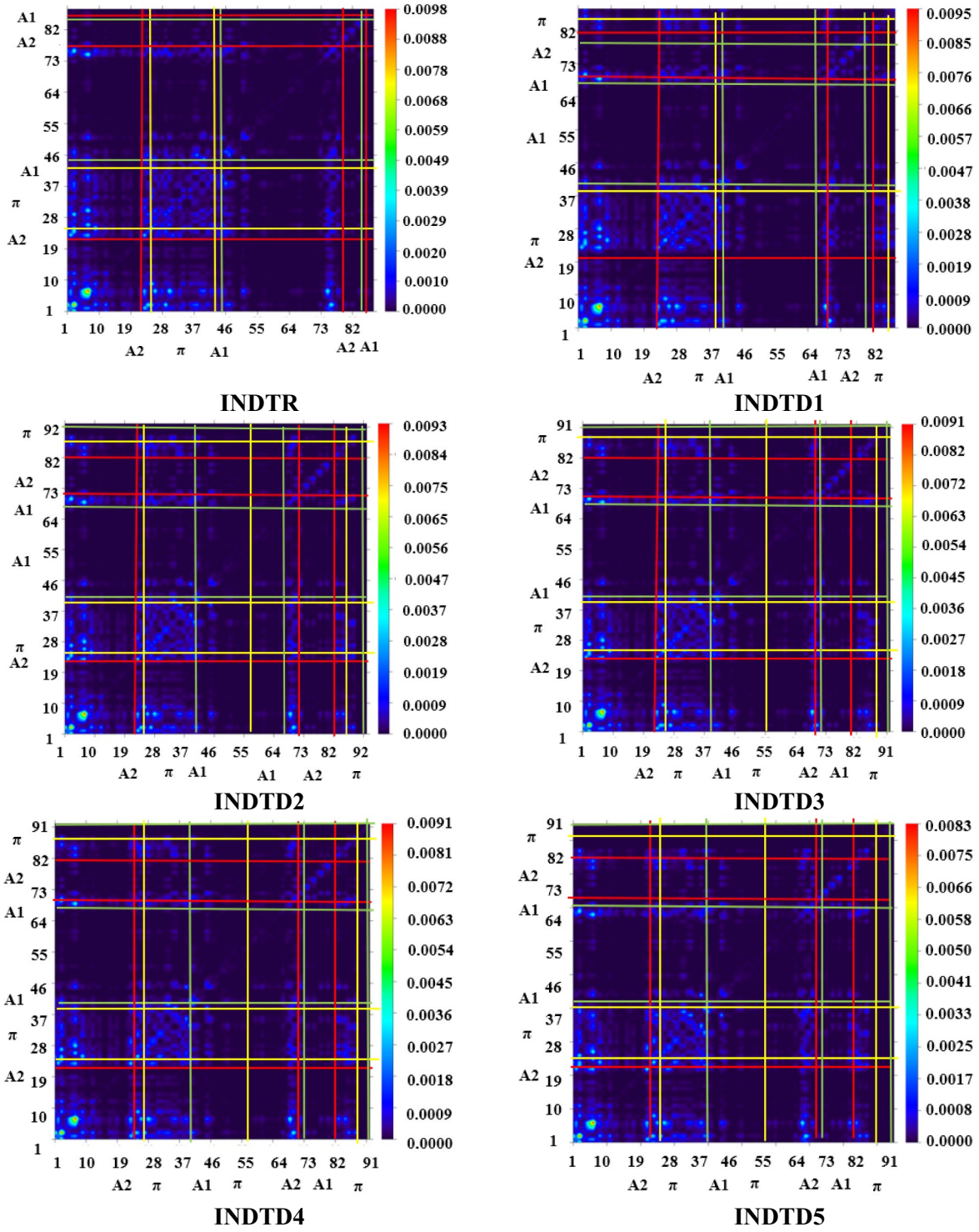

Figure 7. Transition density matrix maps of **INDTR** and **INDTD1**–**INDTD8** compounds.

having E_b values less than 1.9 eV are regarded as highly efficient materials for NF-OSCs[69]. Interestingly, all tailored chromophores reveal lower exciton binding energy values than 1.9 eV and also lesser than the reference chromophore. The aforesaid chromophores with low E_b enable easier exciton dissociation and rapid charge flow which in turn increases current charge density and makes them favorable optoelectronic materials. Therefore, among all modified compounds, **INDTD7** and **INDTD5** have lower E_b values and exhibit efficient charge mobility and photovoltaic properties owing to their greater tendency of exciton dissociation.

Hole–electron analysis

Hole–electron analysis is effectively performed using the Multiwfn 3.7 software[29] in order to determine the mobility of holes and electrons in the studied compounds[70]. The dark colors represent the highest density regions

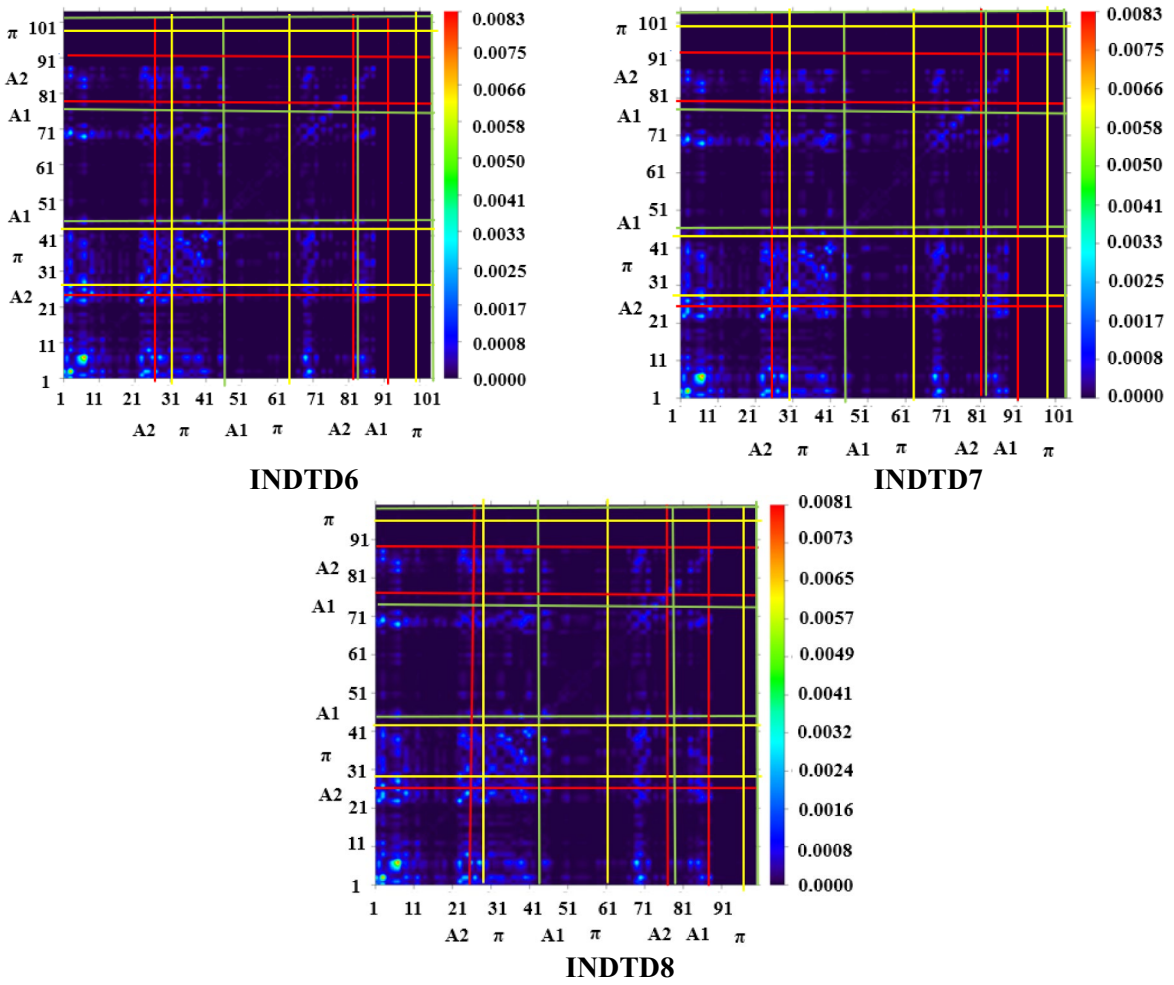

Figure 7. (continued)

Molecules	$E_{H\text{-}L}$ (eV)	E_{opt} (eV)	E_b (eV)
INDTR	2.288	1.711	0.577
INDTD1	2.260	1.685	0.575
INDTD2	2.255	1.680	0.575
INDTD3	2.237	1.664	0.573
INDTD4	2.238	1.665	0.573
INDTD5	2.187	1.631	0.556
INDTD6	2.234	1.663	0.571
INDTD7	2.183	1.629	0.554
INDTD8	2.190	1.626	0.564

Table 4. Calculated binding energies of the studied compounds.

while the light colors indicate lowest density regions on vertical axis in the entitled graphs. Figure 8 shows that the hole intensity in the **INDTR** compound is highest at the C23 and C25 atoms in the π–spacer region, while the electron intensity is maximum at C45 and C46 atoms within the end-capped acceptor. Nevertheless, it is observed that in all modulated compounds hole intensity is maximum at different atoms of carbon present in the π-linker unit, while electron intensity is higher at various atoms of carbon present in the terminal acceptor region owing to the presence of robust electron withdrawing moieties attached to the terminal acceptors.

Remarkably, in **INDTD8** chromophore, where the sulphonic acid ($-SO_3H$) groups are substituted with nitro ($-NO_2$) groups, enhances electron density at the nitrogen atoms and significant charge transfer occurs due to resonance and robust electron-withdrawing effects. In general, **INDTR** and **INDTD1–INDTD4** chromophores appear to be electron-type materials, while **INDTD5–INDTD8** chromophores emerge to be hole-type materials. This is because maximum charge density is observed in both electronic as well as hole bands as presented in

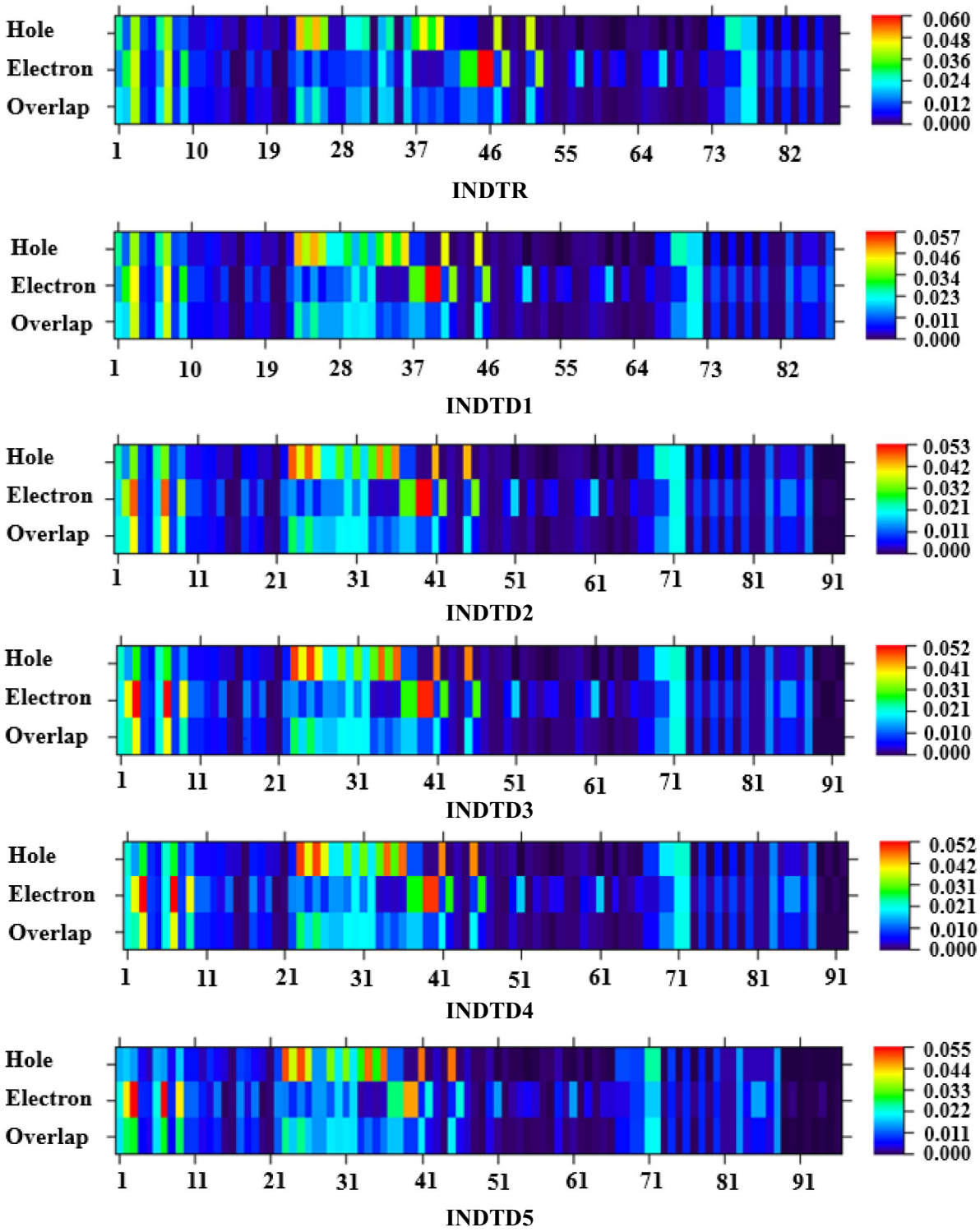

Figure 8. Electron and hole maps of **INDTR** and **INDTD1**–**INDTD8** compounds.

the Fig. 8. Furthermore, charge transfer in the studied compounds is manifested by the electron–hole coupling. The descending trend of charge displacement via electron–hole coupling in all the examined compounds is as follows: **INDTD8** > **INDTD7** > **INDTD5** > **INDTD6** > **INDTD4** > **INDTD3** > **INDTD2** > **INDTD1** > **INDTR**. This declining pattern indicates that electron–hole coupling is greater in **INDTD8**, **INDTD7** and **INDTD5** chromophores than the **INDTR** chromophore. Consequently, all designed derivatives exhibit significant charge transfer and therefore regarded as efficient optoelectronic materials.

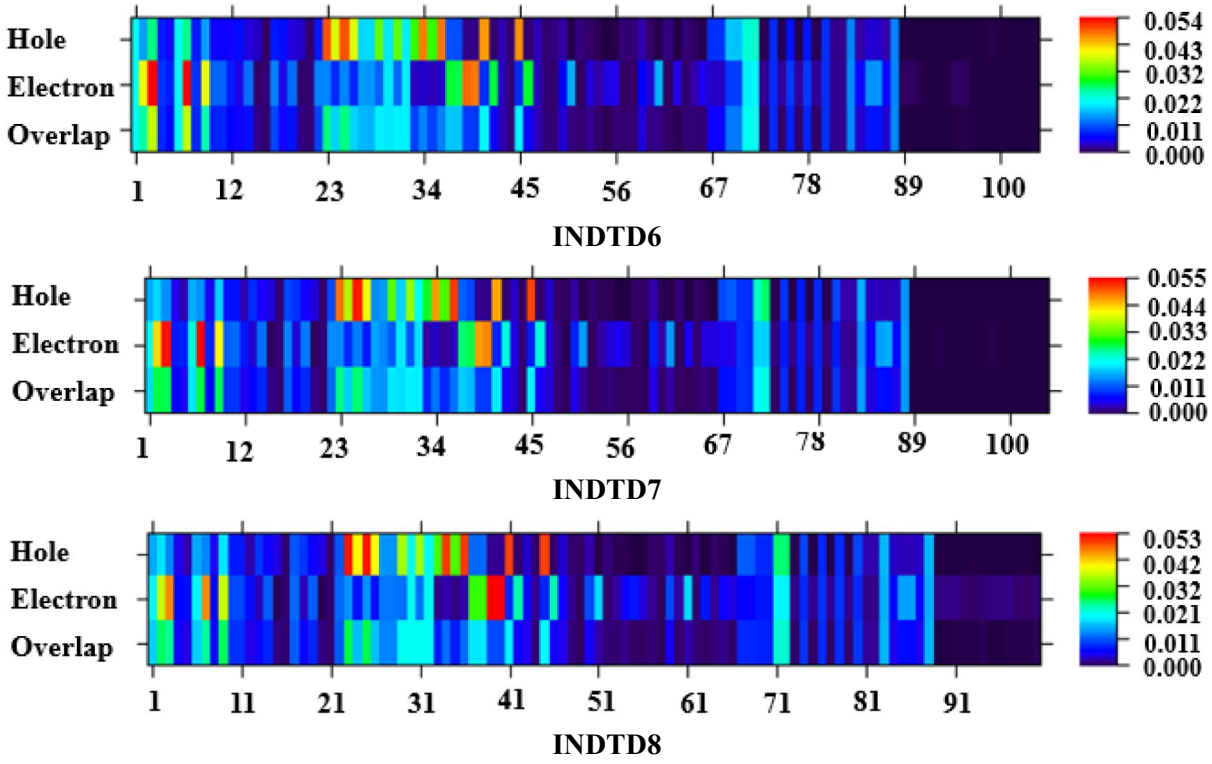

Figure 8. (continued)

Open circuit voltage (V_{oc})

The open-circuit voltage (V_{oc}) is known as the maximum voltage delivered by a solar cell device to an external load at zero current[71]. One of the challenging aspects to achieve high-performance OSCs is to obtain high open-circuit voltage (V_{oc}). It is known from the literature analysis that the most efficient OSCs have attained the V_{oc} in the range of 0.8–0.9 V along with a large energy loss of > 0.5 eV[72,73]. Moreover, the V_{oc} plays a key role in determining the power conversion efficiency (PCE). Hence, to achieve high PCE, the understanding of V_{oc} and E_{loss} is indispensable[74,75]. Various influencing parameters are present which can affect the V_{oc} among which the most revealing are the distribution of charge transfer (CT) states, DOS distribution, infra-structure and donor–acceptor (D–A) interface area. There are certain scaling factors for the measurement of V_{oc} for a solar cell. These are HOMO of the donor and LUMO of an acceptor compound. Mathematically, the V_{oc} is measured as the energy difference of the HOMO of donor and the LUMO of acceptor stated by the Scharber's Equation[76].

$$V_{oc} = I/e(|E^{D}_{HOMO}| - |E^{A}_{LUMO}|) - 0.3. \quad (2)$$

The 0.3 is a constant value which is known as voltage drop[77].

In this study, the characterization of **INDTR** and **INDTD1–INDTD8** are performed to observe their V_{oc} at the afore-said level of DFT. According to the molecular nature of the investigated molecules, **PTB7** donor polymer is selected for establishing the donor–acceptor blend and to specifically align their energy levels. The E_{HOMO} of **PTB7** is – 6.467 eV and E_{LUMO} is – 1.685 eV. Similarly, the energy gap between its HOMO and LUMO is 4.782 eV. The literature analysis shows that E_{LUMO} of the donor must be higher that E_{LUMO} of the acceptor for efficient charge mobility. Hence, E_{LUMO} of the designed acceptors (**INDTR** and **INDTD1–INDTD8**) are as follows: – 3.505, – 3.506, – 3.539, – 3.579, – 3.576, – 3.705, – 3.583, – 3.715 and – 3.729 eV, respectively which are lower than that of **PTB7**. Figure S4 depicts the formation pattern of these chromophores with the donor polymer (**PTB7**). The calculated results show that these compounds exhibit significant V_{oc} values. The reason for the prominent results is the end-capped tailoring with efficient acceptor moieties. The following decreasing order is obtained for V_{oc} among the titled chromophores: **INDTR > INDTD1 > INDTD3 > INDTD4 > INDTD3 > IND TD6 > INDTD5 > INDTD7 > INDTD8** (Table S33).

Literature shows that the theoretically calculated values of V_{oc} for the non-fullerene acceptor compounds are reported higher than the experimental values of V_{oc} as reported in the case of ternary OSCs incorporating 2TT unit i.e., thiophene [3,2-b] thiophene (TT) with V_{oc} value of 1.04 V which is lower[2] than theoretically calculated values of **INDTD1–INDTD8** compounds. It is expected that this research may facilitate in achieving improved optoelectronic and photovoltaic properties from the newly designed acceptor compounds. Moreover, this analysis may support their future synthesis for the next-generation photovoltaics.

Fill factor and power conversion efficiency

The performance of a solar cell (SC) device is largely examined by the key factors such as fill factor (FF), open circuit voltage (V_{oc}) and short circuit current density (J_{sc})[78]. Thus, the FF for the studied compounds is theoretically estimated by using the following Equation.

$$FF = \frac{\frac{eV_{oc}}{KBT} - \ln\left[\frac{eV_{oc}}{KBT} + 0.72\right]}{\frac{eV_{oc}}{KBT} + 1}. \quad (3)$$

The parameter such as $\frac{eV_{oc}}{KBT}$ signifies the normalized voltage. While, "e" is known as the elementary charge which is fixed at 1. K_B and T are Boltzmann constant (1.380649×10^{-23} J per kelvin) and temperature (300 K), respectively.

Among the designed compounds, highest FF is obtained for **INDTD2** (0.954) as compared to other derivatives as shown the Table S34. Similarly, another significant metric which is known as the power conversion efficiency (PCE) is calculated using the Eq. (4) which is as follows:

$$PCE = \frac{J_{sc} V_{oc} FF}{P_{in}}. \quad (4)$$

The P_{in} is known as the incident power from approaching light source which is inversely related to the PCE of a photovoltaic material. It is known from the literature that J_{sc} value largely influences the band gaps and charge transfer rates of a particular molecule[79]. From the above-mentioned Equation, a reasonable approximation of PCE is made which showed that it is found in a range of 31.77–36.91% and the highest PCE is observed for **INDTD1** (36.91%). Moreover, all derivatives show comparable PCEs with the **INDTR** reference (36.63%). Thus, the proposed organic compounds are significant candidates for development of efficient photovoltaic materials.

Conclusion

In summary, new non-fullerene acceptors (**INDTR** and **INDTD1–INDTD8**) are proposed systematically to explore their optoelectronic and photovoltaic characteristics by utilizing the quantum chemical approach. The designed derivatives showed lower band gaps (2.183–2.269 eV) and bathochromic shifts in solvent such as 735.937–762.318 nm. Interestingly, the most significant results are obtained for **INDTD5**, **INDTD7** and **INDTD8** chromophores as compared to other compounds. The compounds (**INDTD5**, **INDTD7** and **INDTD8**) showed least energy gaps (2.187, 2.183 and 2.190 eV, respectively) and binding energies (0.556, 0.554 and 0.564 eV, respectively) which are indicative of efficient charge mobility and higher exciton dissociation rates, respectively. Moreover, these chromophores also exhibited the highest absorption values in the UV–Vis spectra 760.354, 760.914 and 762.318 nm, correspondingly. Furthermore, the investigated molecules are blended with the donor polymer (**PTB7**) for the sake of photovoltaic insights and showed good results for V_{oc}, FF and PCEs. The hole–electron analysis rendered effective charge mobilities in entitled chromophores. These DFT analyses for the studied compounds demonstrate that the end-capping strategy adopted for designing the indolonaphthyridine core-based NFAs is significant in attaining efficient photovoltaic features.

Data availability

All data generated or analyzed during this study are included in this published article and its supplementary information files.

Received: 28 June 2024; Accepted: 16 August 2024
Published online: 27 August 2024

References

1. Hu, Y., Wang, J., Yan, C. & Cheng, P. The multifaceted potential applications of organic photovoltaics. *Nat. Rev. Mater.* **7**, 836–838 (2022).
2. Lu, H. *et al.* High-efficiency binary and ternary organic solar cells based on novel nonfused-ring electron acceptors. *Adv. Mater.* **36**, 2307292. https://doi.org/10.1002/adma.202307292 (2024).
3. Chaisson, M. J. *et al.* Multi-platform discovery of haplotype-resolved structural variation in human genomes. *Nat. Commun.* **10**, 1784 (2019).
4. Mahmood, A. Photovoltaic and charge transport behavior of diketopyrrolopyrrole based compounds with A–D–A–D–A skeleton. *J. Clust. Sci.* **30**, 1123–1130 (2019).
5. Xiao, B. *et al.* Quinoxaline-containing nonfullerene small-molecule acceptors with a linear A_2–A_1-D-A_1-A_2 skeleton for poly(3-hexylthiophene)-based organic solar cells. *ACS Appl. Mater. Interfaces* **10**, 10254–10261. https://doi.org/10.1021/acsami.8b00216 (2018).
6. Cui, Y. *et al.* 100 cm^2 organic photovoltaic cells with 23% efficiency under indoor illumination. *Chin. J. Polym. Sci.* **40**, 979–988 (2022).
7. Waqas, M. *et al.* Theoretical framework for achieving high V oc in non-fused non-fullerene terthiophene-based end-capped modified derivatives for potential applications in organic photovoltaics. *RSC Adv.* **13**, 7535–7553 (2023).
8. Zhang, G. *et al.* Renewed prospects for organic photovoltaics. *Chem. Rev.* **122**, 14180–14274. https://doi.org/10.1021/acs.chemrev.1c00955 (2022).
9. Li, X. *et al.* Simplified synthetic routes for low cost and high photovoltaic performance n-type organic semiconductor acceptors. *Nat. Commun.* **10**, 519. https://doi.org/10.1038/s41467-019-08508-3 (2019).
10. Zhang, Y. *et al.* Recent progress of Y6-derived asymmetric fused ring electron acceptors. *Adv. Funct. Mater.* **32**, 2205115. https://doi.org/10.1002/adfm.202205115 (2022).
11. Asif, A. *et al.* Efficient side-chain engineering of thieno-imidazole salt-based molecule to boost the optoelectronic attributes of organic solar cells: A DFT approach. *J. Mol. Graph. Model.* **121**, 108428. https://doi.org/10.1016/j.jmgm.2023.108428 (2023).

12. Fallon, K. J. & Bronstein, H. Indolonaphthyridine: A versatile chromophore for organic electronics inspired by natural indigo dye. *Acc. Chem. Res.* **54**, 182–193. https://doi.org/10.1021/acs.accounts.0c00601 (2021).
13. Stahl, T. *et al.* Tunable semiconducting polymer nanoparticles with INDT-based conjugated polymers for photoacoustic molecular imaging. *Bioconj. Chem.* **28**, 1734–1740. https://doi.org/10.1021/acs.bioconjchem.7b00185 (2017).
14. Fallon, K. J. *et al.* Indolo-naphthyridine-6,13-dione thiophene building block for conjugated polymer electronics: Molecular origin of ultrahigh n-type mobility. *Chem. Mater.* **28**, 8366–8378. https://doi.org/10.1021/acs.chemmater.6b03671 (2016).
15. Fallon, K. J. *et al.* Exploiting excited-state aromaticity to design highly stable singlet fission materials. *J. Am. Chem. Soc.* **141**, 13867–13876. https://doi.org/10.1021/jacs.9b06346 (2019).
16. Purdy, M. *et al.* Synthesis of asymmetric indolonaphthyridines with enhanced excited state charge-transfer character. *J. Mater. Chem. C* **10**, 10742–10747 (2022).
17. Bedi, A. & Zade, S. S. Electrochemical route to solution-processable polymers of thiophene/selenophene capped didodecyloxybenzo[1,2-*b*:4,3-*b*′]dithiophene and their optoelectronic properties. *Macromolecules* **46**, 8864–8872. https://doi.org/10.1021/ma401853q (2013).
18. Ashraf, R. S. *et al.* Chalcogenophene comonomer comparison in small band gap diketopyrrolopyrrole-based conjugated polymers for high-performing field-effect transistors and organic solar cells. *J. Am. Chem. Soc.* **137**, 1314–1321. https://doi.org/10.1021/ja511984q (2015).
19. Zhao, X. *et al.* Double asymmetric core optimizes crystal packing to enable selenophene-based acceptor with over 18% efficiency in binary organic solar cells. *Angew. Chem. Int. Ed.* **62**, e202216340. https://doi.org/10.1002/anie.202216340 (2023).
20. Te Vrugt, M., Löwen, H. & Wittkowski, R. Classical dynamical density functional theory: From fundamentals to applications. *Adv. Phys.* **69**, 121–247. https://doi.org/10.1080/00018732.2020.1854965 (2020).
21. Liang, J., Feng, X., Hait, D. & Head-Gordon, M. Revisiting the performance of time-dependent density functional theory for electronic excitations: Assessment of 43 popular and recently developed functionals from rungs one to four. *J. Chem. Theory Comput.* **18**, 3460–3473. https://doi.org/10.1021/acs.jctc.2c00160 (2022).
22. Frisch, M. J. G. *et al. Gaussian 09* (Gaussian Inc, 2009).
23. Zhao, Y. & Truhlar, D. G. The M06 suite of density functionals for main group thermochemistry, thermochemical kinetics, noncovalent interactions, excited states, and transition elements: Two new functionals and systematic testing of four M06-class functionals and 12 other functionals. *Theor. Chem. Acc.* **120**, 215–241. https://doi.org/10.1007/s00214-007-0310-x (2008).
24. Del Bene, J. E., Aue, D. H. & Shavitt, I. Stabilities of hydrocarbons and carbocations. 1. A comparison of augmented 6–31G, 6–311G, and correlation consistent basis sets. *J. Am. Chem. Soc.* **114**, 1631–1640 (1992).
25. Dennington, R., Keith, T. & Millam, J. G. *6.0.16* (Semichem Inc., 2016).
26. Hanwell, M. D. *et al.* Avogadro: An advanced semantic chemical editor, visualization, and analysis platform. *J. Cheminform.* **4**, 17. https://doi.org/10.1186/1758-2946-4-17 (2012).
27. Stevenson, K. J. Review of originpro 8.5. *J. Am. Chem. Soc.* **133**, 5621 (2011).
28. O'boyle, N. M., Tenderholt, A. L. & Langner, K. M. cclib: A library for package-independent computational chemistry algorithms. *J. Comput. Chem.* **29**, 839–845. https://doi.org/10.1002/jcc.20823 (2008).
29. Lu, T. & Chen, F. Multiwfn: A multifunctional wavefunction analyzer. *J. Comput. Chem.* **33**, 580–592. https://doi.org/10.1002/jcc.22885 (2012).
30. O'boyle, N. M. cclib: A library for package-independent computational chemistry algorithms. *J. Comput. Chem.* https://doi.org/10.1002/jcc.20823 (2022).
31. Zhurko, G. A. & Zhurko, D. A. *ChemCraft, Version 1.6*. http://www.Chemcraftprog.com (2009).
32. Al-Temimei, F. A. & Mraity, H. A. A. DFT/TD-DFT investigation of novel D–π–A configuration dyes for improving solar cell efficiency. *Struct. Chem.* **33**, 859–869 (2022).
33. Bourass, M. *et al.* DFT and TD-DFT calculation of new thienopyrazine-based small molecules for organic solar cells. *Chem. Central J.* **10**, 1–11 (2016).
34. Woodward, R. B. & Hoffmann, R. The conservation of orbital symmetry. *Angew. Chem. Int. Ed. Engl.* **8**, 781–853. https://doi.org/10.1002/anie.196907811 (1969).
35. Orbitals, I. F. F. *Organic Chemical Reactions, Reference Edition* Vol. 256, 368 (Wiley, 1976).
36. Yu, J., Su, N. Q. & Yang, W. Describing chemical reactivity with frontier molecular orbitalets. *JACS Au* **2**, 1383–1394. https://doi.org/10.1021/jacsau.2c00085 (2022).
37. Pathade, V. A., Waghchaure, R. H., Jagdale, B. S., Pawar, T. B. & Pathade, S. S. Molecular structure, frontier molecular orbital and spectroscopic examination on dihydropyrimidinones: A comparative computational approach. *J. Adv. Sci. Res.* **11**, 64–70 (2020).
38. Golding Sheeba, G., Usha, D., Amalanathan, M., Sony Michael Mary, M. & MarshanRobert, H. Molecular structure, vibrational spectroscopic, frontier molecular orbital and natural bond orbital analysis of anti-cancer drug 6-chloro-3-pyridine carbonitrile. *Spectrosc. Lett.* **54**, 419–436. https://doi.org/10.1080/00387010.2021.1932964 (2021).
39. Adnan, M. *et al.* Molecular modelling of fused heterocycle-based asymmetric non-fullerene acceptors for efficient organic solar cells. *J. Saudi Chem. Soc.* **27**, 101739. https://doi.org/10.1016/j.jscs.2023.101739 (2023).
40. Sivakumar, G., Paramasivam, M., Bharath, D. & Rao, V. J. Energy level tuning of 'Z'-shaped small molecular non-fullerene electron acceptors based on a dipyrrolo[2,3-*b* :2′,3′-*e*]pyrazine-2,6(1 *H*,5 *H*)-dione acceptor unit for organic photovoltaic applications: A joint experimental and DFT investigation on the effect of fluorination. *New J. Chem.* **43**, 5173–5186. https://doi.org/10.1039/C8NJ05645E (2019).
41. Li, W., Wang, Q., Cui, F. & Jiang, G. Covalent organic framework with sulfonic acid functional groups for visible light-driven CO2 reduction. *RSC Adv.* **12**, 17984–17989. https://doi.org/10.1039/d2ra02660k (2022).
42. Kim, S.-Y., Kim, J. H., Choi, M.-W. & Park, S. Y. A novel n-type organic semiconductor comprising a 1,5-naphthyridine-2,6-dione unit. *J. Mater. Chem. C* **10**, 17703–17713. https://doi.org/10.1039/D2TC03882J (2022).
43. Parr, R. G., Donnelly, R. A., Levy, M. & Palke, W. E. Electronegativity: The density functional viewpoint. *J. Chem. Phys.* **68**, 3801–3807 (1978).
44. Politzer, P. & Truhlar, D. G. (eds) *Chemical Applications Ofnlomic and Molecular Electrostatic Potentials* (Plenum Press, 1981).
45. Parr, R. G. & Pearson, R. G. Absolute hardness: Companion parameter to absolute electronegativity. *J. Am. Chem. Soc.* **105**, 7512–7516. https://doi.org/10.1021/ja00364a005 (1983).
46. Parthasarathi, R., Padmanabhan, J., Elango, M., Subramanian, V. & Chattaraj, P. K. Intermolecular reactivity through the generalized philicity concept. *Chem. Phys. Lett.* **394**, 225–230 (2004).
47. Chattaraj, P. K. & Roy, D. R. Update 1 of: Electrophilicity index. *Chem. Rev.* **107**, 46–74. https://doi.org/10.1021/cr078014b (2007).
48. Pant, D., Darla, N. & Sitha, S. Theoretical assessment of the influences of aromatic bridges on molecular second order nonlinear optical responses of donor-bridge-acceptor types of molecular organic chromophores. *Comput. Theor. Chem.* **1207**, 113522. https://doi.org/10.1016/j.comptc.2021.113522 (2022).
49. Fukui, K. Role of frontier orbitals in chemical reactions. *Science* **218**, 747–754 (1982).
50. Shafiq, F., Mubarik, A., Rafiq, M. & Alshehri, S. M. Star-shaped small donor molecules based on benzotriindole for efficient organic solar cells: A DFT study. *J. Mol. Model.* **30**, 76. https://doi.org/10.1007/s00894-024-05870-y (2024).
51. Hassan, A. U. *et al.* Correlating the charge density and structural fabrication of new organic dyes to create visible light harvesting materials with tunable NLO refining: Insights from DFT. *Chem. Pap.* **77**, 6183–6202. https://doi.org/10.1007/s11696-023-02931-z (2023).

52. Parr, R. G., Szentpály, L. V. & Liu, S. Electrophilicity index. *J. Am. Chem. Soc.* **121**, 1922–1924. https://doi.org/10.1021/ja983494x (1999).
53. Chattaraj, P. K., Sarkar, U. & Roy, D. R. Electrophilicity index. *Chem. Rev.* **106**, 2065–2091. https://doi.org/10.1021/cr040109f (2006).
54. Vijayaraj, R., Subramanian, V. & Chattaraj, P. K. Comparison of global reactivity descriptors calculated using various density functionals: A QSAR perspective. *J. Chem. Theory Comput.* **5**, 2744–2753. https://doi.org/10.1021/ct900347f (2009).
55. Al-Temimei, F. A. Design high—efficiency organic dyes based on fluorescein toward dye—Sensitized solar cells: A DFT/TD-DFT study. *Opt. Quant. Electron.* **54**, 600 (2022).
56. Setsoafia, D. D. Y., Ram, K. S., Mehdizadeh-Rad, H., Ompong, D. & Singh, J. Density functional theory simulation of dithienothiophen [3, 2-b]-pyrrolobenzothiadiazole-based organic solar cells. *Energies* **17**, 313 (2024).
57. Mróz, M. M. *et al.* Long-living optical gain induced by solvent viscosity in a push–pull molecule. *Phys. Chem. Chem. Phys.* **18**, 18289–18296 (2016).
58. Talluri, B., Prasad, E. & Thomas, T. Impact of solvent on the formation and optical properties of digestively ripened, ultra-small ($r < 2$ nm) copper oxide quantum dots. *J. Mol. Liq.* **265**, 771–778. https://doi.org/10.1016/j.molliq.2018.05.069 (2018).
59. Holtomo, O., Nsangou, M., Fifen, J. J. & Motapon, O. DFT study of the solvent effects on the structure, UV–Vis spectra and the antioxidant activity of caffeic acid phenethyl ester and some of its derivatives. *J. Chem. Chem. Eng.* **7**, 910 (2013).
60. Tai, K. *et al.* A comparison of physicochemical and functional properties of icaritin-loaded liposomes based on different surfactants. *Colloids Surf. A Physicochem. Eng. Asp.* **518**, 218–231 (2017).
61. Ans, M. *et al.* Designing three-dimensional (3D) non-fullerene small molecule acceptors with efficient photovoltaic parameters. *ChemistrySelect* **3**, 12797–12804. https://doi.org/10.1002/slct.201802732 (2018).
62. Hasan, M. A. & Sumathy, K. Photovoltaic thermal module concepts and their performance analysis: A review. *Renew. Sustain. Energy Rev.* **14**, 1845–1859 (2010).
63. Goszczycki, P., Stadnicka, K., Brela, M. Z., Grolik, J. & Ostrowska, K. Synthesis, crystal structures, and optical properties of the π–π interacting pyrrolo [2, 3-b] quinoxaline derivatives containing 2-thienyl substituent. *J. Mol. Struct.* **1146**, 337–346 (2017).
64. Ans, M. *et al.* Designing alkoxy-induced based high performance near infrared sensitive small molecule acceptors for organic solar cells. *J. Mol. Liq.* **305**, 112829 (2020).
65. Majeed, M. *et al.* Modified optoelectronic parameters by end-group engineering of ADA type non-fullerene-based small symmetric acceptors constituting IBDT core for high-performance photovoltaics. *J. Phys. Chem. Solids* **181**, 111495 (2023).
66. Ans, M., Iqbal, J., Ayub, K., Ali, E. & Eliasson, B. Spirobifluorene based small molecules as an alternative to traditional fullerene acceptors for organic solar cells. *Mater. Sci. Semicond. Process.* **94**, 97–106 (2019).
67. Köse, M. E. Evaluation of acceptor strength in thiophene coupled donor–acceptor chromophores for optimal design of organic photovoltaic materials. *J. Phys. Chem. A* **116**, 12503–12509. https://doi.org/10.1021/jp309950f (2012).
68. Dkhissi, A. Excitons in organic semiconductors. *Synth. Metals* **161**, 1441–1443 (2011).
69. Kim, B., Zhen, C., Jeong, E. J., Kieffer, J. & Kim, J. Organic dye design tools for efficient photocurrent generation in dye-sensitized solar cells: Exciton binding energy and electron acceptors. *Adv. Funct. Mater.* **22**, 1606–1612. https://doi.org/10.1002/adfm.201101961 (2012).
70. Mehboob, M. Y., Hussain, R., Irshad, Z. & Adnan, M. Enhancement in the photovoltaic properties of hole transport materials by end-capped donor modifications for solar cell applications. *Bull. Korean Chem. Soc.* **42**, 597–610. https://doi.org/10.1002/bkcs.12238 (2021).
71. Mehboob, M. Y. *et al.* Designing N-phenylaniline-triazol configured donor materials with promising optoelectronic properties for high-efficiency solar cells. *Comput. Theor. Chem.* **1186**, 112908 (2020).
72. Wei, Y. *et al.* Binary organic solar cells breaking 19% via manipulating the vertical component distribution. *Adv. Mater.* **34**, 2204718. https://doi.org/10.1002/adma.202204718 (2022).
73. Sun, R. *et al.* Single-junction organic solar cells with 19.17% efficiency enabled by introducing one asymmetric guest acceptor. *Adv. Mater.* **34**, 2110147. https://doi.org/10.1002/adma.202110147 (2022).
74. Al-Temimei, F. A. & Hameed, B. S. Theoretical investigation of new series diphenylsulfone derivatives suitable candidates for organic light-emitting diodes (OLEDS) applications. *Struct. Chem.* **35**, 161–179. https://doi.org/10.1007/s11224-023-02202-3 (2024).
75. Abdali, S. A., Al-Temimei, F. A. & Al-Abbas, S. S. Computational design of D-π-A dyes for improved photovoltaic performance: A DFT approach. *J. Comput. Electron.* **23**, 209–223. https://doi.org/10.1007/s10825-024-02131-2 (2024).
76. Wazzan, N. A. A DFT/TDDFT investigation on the efficiency of novel dyes with ortho-fluorophenyl units (A1) and incorporating benzotriazole/benzothiadiazole/phthalimide units (A2) as organic photosensitizers with D-A2–π–A1 configuration for solar cell applications. *J. Comput. Electron.* **18**, 375–395. https://doi.org/10.1007/s10825-019-01308-4 (2019).
77. Mehboob, M. Y. *et al.* Quantum chemical design of near-infrared sensitive fused ring electron acceptors containing selenophene as π-bridge for high-performance organic solar cells. *J. Phys. Org. Chem.* **34**, e4204. https://doi.org/10.1002/poc.4204 (2021).
78. Brus, V. V. *et al.* Solution-processed semitransparent organic photovoltaics: From molecular design to device performance. *Adv. Mater.* **31**, 1900904. https://doi.org/10.1002/adma.201900904 (2019).
79. Hussain, R. *et al.* Role of novel carbon–oxygen-bridged Z-shaped non-fullerene acceptors for high efficiency organic solar cells. *Synth. Metals* **290**, 117159. https://doi.org/10.1016/j.synthmet.2022.117159 (2022).

Acknowledgements

Dr. Muhammad Khalid gratefully acknowledges the financial support of HEC Pakistan (Project No. 20-14703/NRPU/R&D/HEC/2021). Authors are thankful for cooperation and collaboration of A.A.C.B from IQ-USP, Brazil especially for his continuous support and providing computational lab facilities. A.A.C.B. (Grant 2015/01491-3) is highly thankful to Fundação de Amparo à Pesquisa do Estado de São Paulo for the cooperation and financial assistance. Authors also thank Researchers Supporting Project number (RSPD2024R645), King Saud University, Riyadh, Saudi Arabia.

Author contributions

Mashal Khan: Conceptualization; methodology; supervision. Muhammad Khalid: Data curation; formal analysis. Shahzad Murtaza: Methodology; software; project administration. Ataualpa Albert Carmo Braga: Data curation; formal analysis. Khalid Abdullah Alrashidi: Resources; software; supervision. Sarfraz Ahmed: Conceptualization; resources; project administration.

Competing interests

The authors declare no competing interests.

Additional information

Supplementary Information The online version contains supplementary material available at https://doi.org/10.1038/s41598-024-70457-9.

Correspondence and requests for materials should be addressed to M.K.

Reprints and permissions information is available at www.nature.com/reprints.

Publisher's note Springer Nature remains neutral with regard to jurisdictional claims in published maps and institutional affiliations.